

A Publication of the Department of Mechanical Engineering, Tezpur University

E-Journal





E-Journal
Department of Mechanical Engineering
Tezpur University

Editorial Board

Dr. Tapan K. Gogoi
Dr. Partha P. Dutta
Dr. P. Kalita
Dr. S. M. Kamal

Editorial

The department of Mechanical Engineering, Tezpur University unveils its first issue of the E-Journal with a vision to provide a scope to the students to publish their innovative ideas/works in the field of Mechanical Engineering and allied areas. The main idea of this E-Journal is to publish some of the selective works that have been carried out by the final year B.Tech/M.Tech students as a part of their thesis work. The primary objective of introducing this kind of E-Journal is to make students learn how to write a research paper. The first issue of this E-Journal presents six selective publications based on the project works of B.Tech/M.Tech students carried out during the academic year 2017-2018. We received a total of ten papers. All the papers have been peer-reviewed by the area experts of the department. After receiving the revised version of the papers, the editorial board has selected six papers for publication. The editorial board expresses gratitude to all authors specially the student authors for their valuable contribution, which makes it possible to unveil the first issue of this E-Journal. The editorial board also thanks all the reviewers for providing valuable comments, the incorporation of which improves the quality of the papers. Hope this E-Journal helps the student community of the department of Mechanical Engineering, Tezpur University in improving the presentation skill in written form.

Dr. T. K. Gogoi

Dr. Partha P. Dutta

Dr. P. Kalita

Dr. S. M. Kamal

(Editorial Board Members)

Contents

Title of the paper	Page No.
KHAAT-KHAAT: A Two Legged Single Degree of Freedom Walking Mechanism	1–4
Performance Analysis of Solar Heat Driven Organic Rankine Cycle	5–9
Enhancement of Heat Transfer Rate in Sinusoidal Channel	10–15
Performance Analysis of a Coal Fired Open Cycle MHD Generator	16–27
Performance Analysis of a Coal-fired Reheat Regenerative Steam Power Plant	28–32
Laser Forming Mechanism: A Review	33–35

Tirupati Krishnan Biswas
tirupatibiswas@gmail.com

Amit Kumar
amitmoral44@gmail.com

Satkarsh Maurya
satkarshm@gmail.com

KHAAT-KHAAT: A Two Legged Single Degree of Freedom Walking Mechanism

Abstract— Man has been indulging in the development of humanoid automatons since 19th century. These mechanisms have been helpful in various spheres of life: medical science, military, machining etc. This study focuses on development of a two-legged single degree of freedom walking mechanism. The mechanism works on the principle of four-bar parallel link mechanism. The primary objective of the present is to develop a walking mechanism system which can be controlled using a smart-phone. There exists an ample scope of developing this system further to assist people with special abilities.

Keywords— Walking Mechanism, Four -bar mechanism, Parallelogram, Double Parallelogram mechanism, Arduino board, Bluetooth control

1. Introduction

A great part of the Earth's surface is extremely uneven and so, even with the development of wheeled vehicles, those regions have remained mostly inaccessible. Mountainous regions, ravines, etc. have all posed great challenges to wheeled locomotion. The fact that the highest point on the Earth cannot be reached on wheels proves this. In this age of space exploration, similar terrains on the Moon and other rocky planets have conspired to make wheels ineffective in exploring them. This is where the importance of legs come. Legs can walk over obstacles, climb steep slopes and therefore, are the most suitable for the above mentioned terrains. This is how the thought of developing legged mechanisms came into being.

Presently there has been development of highly advanced legged mechanisms and robots with the help of advanced modern technology. However, man has been trying to make such machines since long ago (resembling human beings). The Greek engineer Ctesibius (c. 270 BC) may be credited to have started the era of robot-like structures. He had applied pneumatics and hydraulics to build water clocks with moving structures that resembled human beings. His work was described in "Mechanical Collection" by his disciple Philo of Byzantium. Based on this, Hero of Alexandria (c. 85 AD) wrote "On Automatic Theatres, On Pneumatics and On Mechanics" which is thought to be the first well documented book describing robots and their mechanisms, which were workable and not based on mythology. Such robots called 'automatos' by the Greeks were made to perform simple repetitive tasks only. The early ninth century saw the acquisition of the Greek texts in monasteries by the Caliph of Baghdad, which led to the development of "Kitab al-Hiyal", a book which described about hundred devices and mechanisms, gathered from those acquired texts. "The Science of

Ingenious Mechanisms" by Badi'as-Zaman Isma'il bin Ar-Razzaz Al-Jazari compiled the description about all the known mechanisms from the past and the present and some inventions of the author and so is regarded as a significant treatise of the eleventh century. Most of the inventions described by Al-Jazari were based on hydraulics and mechanics and resembled Ctesibius's robots. The difference between the Greek and Arab robots was that the Arab robots were more practical and had wide uses, whereas the Greek ones were simpler with only a handful uses. The eighteenth century saw the development of mechanical puppets in Europe. Three figures—the Scribe, the Draftsman and the Musician, built by a Swiss watchmaking industry were entertainment figures, based on highly sophisticated cam mechanisms. These figures acted as an example for Jacques de Vaucanson, who in 1738 built a mechanical duck with multiple cams and one wing contained over 400 small parts. The duck was so designed that it could eat, drink, quack, splash and even defecate. This was one of the best inventions of de Vaucanson, but unfortunately it got lost in the depths of history [1].

Eadweard Muybridge is considered as the pioneer in the field of robots using animal-type locomotion for movement. He studied the movement of 40 different types of mammals, and published his results in the Scientific American Journal in 1878. Using these results, L.A. Rygg in 1893 proposed a quadruped 'The Mechanical Horse' in which the stirrups were used as pedals; the movement was then transmitted to the 'mechanical legs' of the quadruped, which in turn made the quadruped walk [2,3].

In 1997, Shieh et al from the University of Maryland, designed a walking machine with single degree of freedom system and published their results in "Journal Of Robotics Systems". The walking machine used six-bar leg mechanisms with an embedded skew pantograph and

generated a delta-shaped foot-path. Its mechanism was well-designed for climbing stairs or stepping over obstacles [4].

In the recent years, Siddharth S. and Girish A. described the synthesis of a single degree of freedom device in their thesis, which they designed and built in the Ohio State University. The machine is based on the Biped Walking Theory and focuses on helping people with disabilities to walk. The mechanism is a variant of the Jansen's linkage, a planar mechanism. The duo referred to a thesis provided by Brett C. Brown of the same institution, which inspired them to work on the same. Brown described the design of a biped robot with a single degree of freedom system having only one input. His design was based on the Biped Walking Theory and Kinematic Mechanisms Theory [5, 6].

2. Objective

The objective behind taking up this project is to come up with a stable walking mechanism which can be controlled using only one input. A possible extension of our work is related to assisted walking for disabled persons wherein the presently used wheel-chairs can be modified to incorporate the feature, based on our design, which can help it to climb stairs.

3. Methodology

The main principle on which the walking mechanism works is the four bar parallelogram mechanism. It refers to a special type of four bar link mechanism in which the crank and rocker length and coupler and frame length are equal. Thus, it acts like a parallelogram. The four bar parallel link mechanism is shown in the figure below.

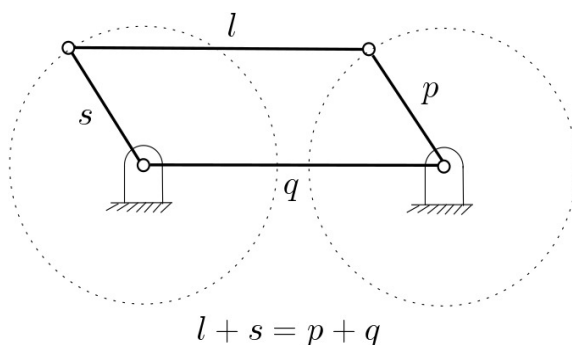


Figure 1 Four-bar parallelogram mechanism

Using this principle has its own advantage and disadvantage. This principle is advantageous due to the fact that the links are always parallel to each other. So, if this mechanism is incorporated in wheel-chairs, the person sitting in it will always remain parallel to the ground, even if the chair is modified to climb stairs. But the disadvantage is that the principle will fail to work if there is any error in dimensions. This is because even a little error in dimensions will not allow the formation of a parallelogram.

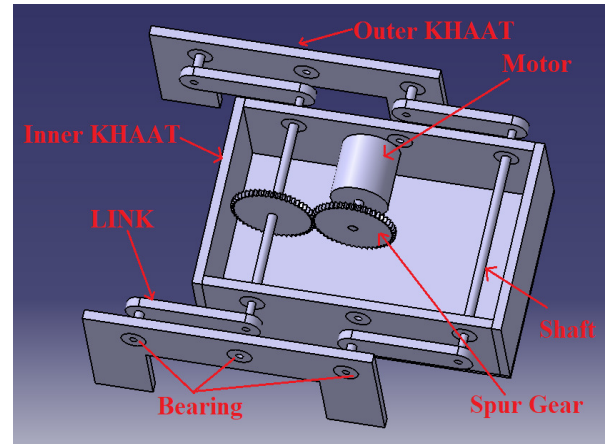


Figure 2 CAD model of the walking mechanism using four-bar parallelogram mechanism

A CAD model of the mechanism is shown in the figure. It can be seen from the figure that there are two bed-like structures in the walking mechanism. These bed-like structures have been named KHAAT based on the Hindi name for bed and connected using parallel links using rotary joints. The mechanism contains two KHAATS, one inside the other. Hence, we call the mechanism KHAAT-KHAAT.

A singular configuration is the position of a mechanism at which its future motion becomes unpredictable, and the forces cannot be determined or they become infinite. It is also known as mechanical singularity. The evaluation of kinematic equations at the mechanical singularity proves worthless as mathematics fails at that point owing to the mysterious behaviour of infinity.

A problem related to singular configuration arises at a point while developing the walking mechanism using a four-bar parallel linkage. At that point, it becomes difficult to say whether the outer Khaat moves parallel to the ground or not. Also, it has been found that end of the outer Khaat exhibit a peculiar motion whereby one end moves upwards and another end moves downwards. This

ultimately violates the formation criteria of a parallelogram, thus indicating the failure of the four-bar parallel mechanism. Thus, we have decided to use a double parallelogram mechanism, which does not necessarily have only four bars, but it works like the parallelogram mechanism, without exhibiting a singular configuration.

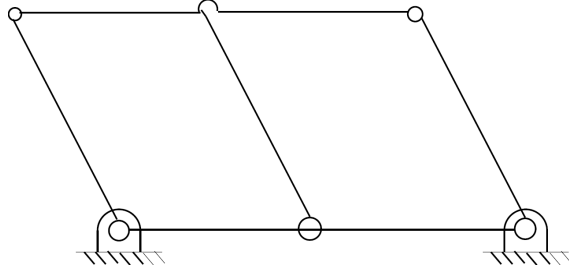


Figure 3 Double parallelogram mechanism

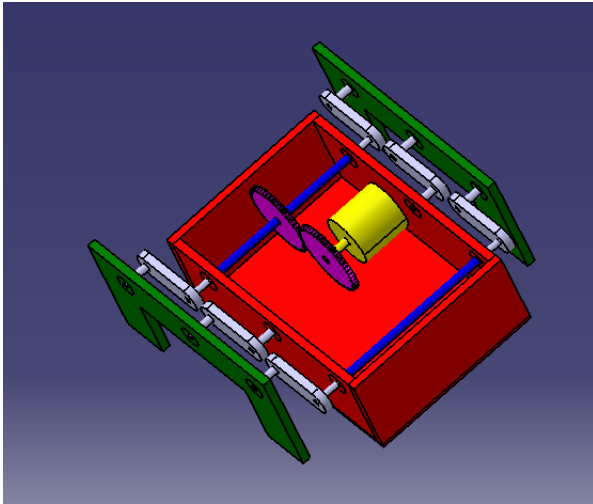


Figure 4 Isometric view (CAD model) of KHAAT-KHAAT

We use translucent and opaque coloured acrylic sheet for designing the body frame of the mechanism. Acrylic is the common name of Poly (methyl methacrylate) (PMMA), a thermoplastic polymer often used in sheet form. It has the chemical form $(C_5O_2H_8)_n$. It has advantages like being lightweight and unlike glass, it is resistant to shatter. It is strong, tough and has better impact strength when compared to glass. These advantages led us to choose it as the material of the body frame. The sheet is cut according to dimensions.

For shafts and connecting links, we use nylon as the material. Nylon rods have been machined in a lathe so as to form the desired shape required. We also require bearings to provide constrained motion to the links.

Bearings are machine elements which provide only the required motion while constraining all other relative motion. It is also used as a friction-reducing machine element. Bearings may be journal bearings, roller bearings, ball bearings, jewel bearings, fluid bearings etc. depending on the source of motion or load support. The bearing that has been used here is a ball bearing of the number 624. Ball bearings are those bearings in which spherical balls are placed in between the stationary and rotating parts of the bearing. Both radial and thrust loads can be handled by these type of bearings, provided the load application is relatively small. The bearings are fitted in holes drilled in the two KHAATS. The connecting links are fitted in these bearings.

Spur gears have been used for transmitting motion. Spur gears are those gears which are mounted on parallel shafts. They have high transmission efficiency and offer constant velocity ratio. They are compact and easy to install. The gear shaft is passed through the gear and the ends of the shaft are fitted in the holes of the small links which connects the Khaats. The motor is positioned in such a way that the motor shaft while holding the smaller gear in place, maintains perfect meshing between the gears.

The controller of the mechanism has been devised with the help of Arduino UNO, L293D microcontroller and a Bluetooth module HC-05. It is devised in such a way that it can be used to control KHAAT-KHAAT from a distance, using a mobile phone.

4. Conclusion

The work focuses on applying the four-bar parallel link mechanism in order to come up with a single degree of freedom walking mechanism. The mechanism, as of now, can be controlled using a smart-phone by any lay person to make it move in forward or backward direction. The work undertaken during this project has helped us to understand the various challenges that one could possibly face while developing such a system. This understanding could further be employed to modify the present-day wheelchairs in such a way that it can climb stairs. However, challenges are huge, but a project of this kind, if taken, would immensely help the people with special abilities.

Acknowledgement

We would like to express obligation towards our supervisor Dr. V.K. Mehta for his constant support and encouragement throughout the semester regarding the project. We would also express our gratitude towards the Department of Mechanical Engineering and its fraternity for providing us with all the facilities and help required for the completion of the project. Lastly, we would also like

to thank Tezpur University for providing us the infrastructure and facilities for all these years.

References

- [1] Silva, M. F., and Tenreiro Machado, J. A historical perspective of legged robots. *Journal of Vibration and Control* 13, 9-10 (2007), 1447-1486.
- [2] Machado, J. T., and Silva, M. F. An overview of legged robots. In *International symposium on mathematical methods in engineering* (2006), MME Press, Ankara, Turkey.
- [3] Raibert, M. H., Legged robots. *Communications of the ACM* 29, 6 (1986), 499-514.
- [4] Shieh, W.B., Tsai, L.W., and Azarm, S. Design and optimization of a one degree-of-freedom six-bar leg mechanism for a walking machine. *Journal of Field Robotics* 14, 12 (1997), 871-880.
- [5] Brown, B. C. Design of a single-degree-of-freedom biped walking mechanism. PhD thesis, The Ohio State University, 2006.
- [6] Tavolieri, C., Ottaviano, E., Ceccarelli, M., and Rienzo, A. Analysis and design of a 1-dof leg for walking machines. In *15th International Workshop on Robotics in Alpe-Adria-Danube Region (RAAD)*, Balatonfured, Hungary, June (2006), pp.15-17.

Performance Analysis of Solar Heat Driven Organic Rankine Cycle

Samiksha Saikia

saikia.samiksha@gmail.com

Tapan Kumar Gogoi

tapan_g@tezu.ernet.in

Abstract— The objective of this work is to analyse the performance of an Organic Rankine Cycle (ORC) driven by Solar energy during the months of February, May, August and November for Tezpur, Assam. In the ORC, five different working fluids (Butane, Neo-pentane, Iso-pentane, R245fa and R245ca) were investigated and it was found that highest net power (7.72 MW) was obtained with R245fa during February. For all ORC fluids, maximum power was obtained during February while the performance was lowest during August.

Keywords— Parabolic Trough Solar Collector, ORC

1. Introduction

Solar energy is a reliable source of energy which can be used to meet the growing energy demands [1] and solve numerous environmental problems such as global warming and depletion of fossil fuels [2]. There are many solar collectors like PTSCs, solar towers and solar dishes that can be used in solar power plants for capturing solar irradiation [3]. PTSCs are however the most mature technology among the existing solar collectors [4] as they are simple in design and can achieve temperatures upto 400°C.

Solar energy can be classified as low grade energy [5] and hence conventional Rankine cycle is not an economical and efficient alternative for conversion of heat from this low grade energy source. A Rankine cycle employing organic compounds like refrigerants rather than water is called Organic Rankine Cycle and it is the most accepted technology for conversion of low-grade heat energy source into mechanical work [2]. Thermodynamic analyses of solar driven Organic Rankine cycle (ORC) have been performed in a number of studies [6-7] and it was found that this cycle is suitable for extracting lower temperature heat sources upto 300°C [8]. The working fluid selection in ORC is crucial to ORC's thermodynamic and economic performance [9-12].

In the present study, a solar energy driven ORC is thermodynamically analysed. The Heat Transfer Fluid (HTF), viz, water absorbs the solar energy in the PTSC and the hot water is stored in a storage tank. The hot water from the storage tank enters the ORC vapour generator to subsequently heat up the organic fluid. A one dimensional (1-D) PTSC model is implemented and this 1-D model is based on energy conservation which incorporates both the optical and the thermal model. Moreover the solar collector is location specific and can take into account seasonal variations. A storage tank is also considered in

the system. In the ORC, five different working fluids (Butane, Neo-pentane, Iso-pentane, R245fa and R245ca)

are considered for comparative performance analysis of the ORC.

2. System Description

Fig. 1 shows the schematic of the solar heat driven ORC. The PTSC consists of the absorber tube, the glass envelope and a number of support brackets. There are 10 collector elements in series in a single row and a total of 300 rows of such collector series are considered. Table I shows the geometrical data of the LS3 type PTSC. Water is used as HTF in the PTSC which is heated and then stored in the storage tank. The hot water from the storage tank is pumped to the ORC where it transfers heat subsequently to the organic fluid in the vapour generator of the ORC and then again exits the vapour generator back to the storage tank.

3. Mathematical Modelling

3.1. Assumptions

The HTF temperature at PTSC inlet is taken 105 °C. The monthly solar irradiance is calculated using ASHRAE model [12]. The storage tank heat loss is taken into consideration through a heat loss coefficient of 0.5 W/m²K. The storage tank is modelled as a cylindrical tank with a diameter to height ratio of 2. The temperatures of organic fluid vapours at turbine inlet are set 20°C less than the hot water inlet temperature. Similarly, a constant 45°C of superheating is considered for all the working fluids in the ORC.

3.2. PTSC modelling

The solar collector model is based on steady state energy balance at each surface (external and internal) of the PTSC cross-section as shown in Fig. 2 [13]. The model assumes that all temperatures, heat fluxes and

thermodynamic properties are uniform around the circumference of the PTSC elements. Also, all heat flux directions shown in Fig.2 are positive. The glass envelope

($\dot{q}_{5,SolAbs}$) and absorber selective coating ($\dot{q}_{3,SolAbs}$) absorbs the incoming solar radiation and conducts portion

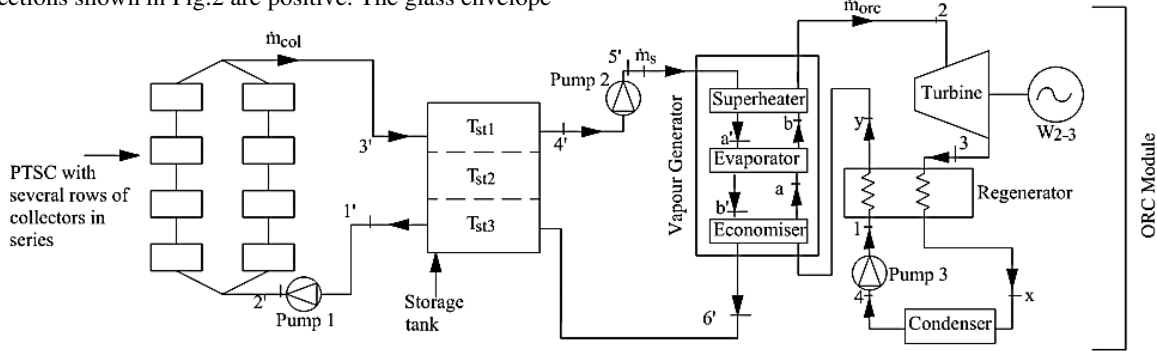


Fig.1 Basic layout of Solar Organic Rankine Cycle

TABLE I
PTSC GEOMETRICAL AND OTHER SYSTEM INPUT PARAMETERS

SOLAR COLLECTOR [13,14]	
Single collector width, W	5.76 m
Single collector length, L	12.27 m
Receiver inner diameter, D_2	0.066 m
Receiver outer diameter, D_3	0.07 m
Cover inner diameter, D_4	0.115 m
Cover outer diameter, D_5	0.121 m
Emittance of the cover, E_5	0.15
Emittance of the receiver, E_3	0.94
Transmittance of the glass cover, τ_{env}	0.96
Reflectivity of the mirror, ρ_{env}	0.94
Absorbance of the receiver, α_{abs}	0.96
Absorbance of the envelope, α_{env}	0.02
Intercept factor, γ	0.93
Volumetric flow rate in a single collector	0.000795 m^3/s
ORC	
Isentropic efficiency of pump, η_p	0.8
Isentropic efficiency of turbine, η_t	0.8
Motor efficiency, η_{motor}	0.8
Generator efficiency, η_{gen}	0.9
Condensation temperature, T_{cond}	30 °C
Regenerator effectiveness, ϵ_{reg}	0.75

of this radiation through the absorber ($\dot{q}_{2-3,cond}$) to the HTF by convection ($\dot{q}_{1-2,conv}$). The remaining solar energy is transmitted back to the glass envelope by convection ($\dot{q}_{3-4,conv}$) and radiation ($\dot{q}_{3-4,rad}$) and lost through conduction in the support brackets ($\dot{q}_{cond,bracket}$). Further, the radiative and convective energy transmitted to the glass envelope is conducted through the glass envelope ($\dot{q}_{4-5,cond}$) and is lost to the environment by convection ($\dot{q}_{5-6,conv}$) and radiation ($\dot{q}_{5-6,rad}$).

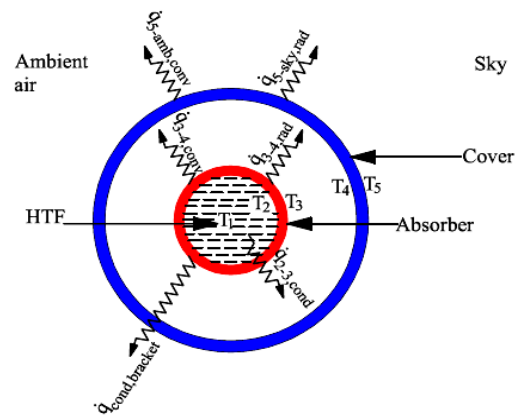


Fig. 2 The heat fluxes with their directions at a given cross-section of the PTSC

The energy balance equations are given below [13].

$$\dot{q}_{1-2,conv} = \dot{q}_{2-3,cond} \quad (1)$$

$$\dot{q}_{3,SolAbs} = \dot{q}_{3-4,conv} + \dot{q}_{3-4,rad} + \dot{q}_{2-3,cond} + \dot{q}_{cond,bracket} \quad (2)$$

$$\dot{q}_{3-4,conv} + \dot{q}_{3-4,rad} = \dot{q}_{4-5,cond} \quad (3)$$

$$\dot{q}_{4-5,cond} + \dot{q}_{5,Solabs} = \dot{q}_{5-6,conv} + \dot{q}_{5-6,rad} \quad (4)$$

The temperature of water at inlet to the PTSC is known. The outlet temperature of the HTF at the exit of each PTSC element is calculated as follows.

$$T_3 = T_2 + \frac{[(\dot{q}_{3,Solabs} - \dot{q}_{3-4,conv} - \dot{q}_{3-4,rad}) - (\dot{m}_{cond,bracket})L]}{\dot{m}_{col}C_p} + \frac{v_{in}^2 - v_{out}^2}{2C_p} \quad (5)$$

3.3. Storage Tank modelling

The storage tank is separated into three mixing zones and the modelling is done as per the procedure outlined in Refs. [15-18]. Three simultaneous linear equations are solved to find the temperature of hot water in the first and second zones of the storage tank (T_{st1} and T_{st2}) and the water temperature at inlet to the storage tank (T_3), T_{st1} and water temperature at outlet from the storage tank (T_4) are set equal while (T_1) is the same with T_{st3} (water temperature in the third zone of the storage tank).

3.4. ORC modelling

The thermodynamic properties of the working fluids (Butane, Neo-pentane, Iso-pentane, R245fa and R245ca) in various states of the ORC are determined using REFPROP 9.0. [19]. Heat loss between the system and surroundings is negligible. Pressure losses in the pipelines and heat exchangers are neglected. The following general mass and energy balance equations of steady flow processes are applied.

Mass balance:

$$\sum \dot{m}_{in} = \sum \dot{m}_{out} \quad (6)$$

Energy balance:

$$\sum \dot{Q} - \sum \dot{W} = \sum (\dot{m}h)_{in} - \sum (\dot{m}h)_{out} \quad (7)$$

Mass flow rate of working fluid in the ORC is calculated using Equation (8).

$$\dot{m}_{ORC} = \frac{\dot{m}_s (h_{5'} - h_{6'})}{h_2 - h_a} \quad (8)$$

where, \dot{m}_s is the mass flow rate of hot water passing through the ORC. \dot{m}_s is set equal to \dot{m}_{col} . Net power and efficiency of the ORC are calculated as

$$Power_{net} = \dot{m}_{ORC} \left[(h_2 - h_3) \eta_{gen} - \left(\frac{h_1 - h_4}{\eta_{motor}} \right) \right] - (\dot{W}_{pump1} + \dot{W}_{pump2}) \quad (9)$$

$$\eta_{ORC} = \frac{Power_{net}}{\dot{m}_{ORC} (h_2 - h_y)} \quad (10)$$

In Equation (9), η_{gen} and η_{motor} are the generator and motor efficiencies. \dot{W}_{pump1} and \dot{W}_{pump2} are the pumping powers required for driving Pump 1 and Pump 2.

4. Results and Discussion

A MATLAB program was developed to simulate the CPC system. The simulation is done for the geographical location of Tezpur, Assam (longitude 92.7926°E and latitude 26.6528°N). The performance of the solar driven CPC system is reported for four months viz. February, May, August and November. The system is considered to operate in the solar storage mode only and the results correspond to the 21st day of each month at a local time of 11 am.

Table II shows the performance variation of ORC along with monthly global irradiation for Tezpur, water temperatures at the PTSC outlet (T_3), storage tank outlet (inlet to ORC vapour generator) (T_5) and ORC generator outlet (inlet to the storage tank) (T_6) for the four months considered. The global solar irradiation is highest during February as a consequence of which the outlet temperature of the HTF from PTSC, power output and efficiency of the ORC is also the maximum during this month. The least power from this system was observed during the month of August. Thus, higher the global irradiation, higher is the outlet temperature of the HTF (water) and so better is the ORC performance.

TABLE II
SOLAR IRRADIATION, WATER TEMPERATURES AT THE PTSC OUTLET (T_3), STORAGE TANK OUTLET (INLET TO ORC VAPOUR GENERATOR) (T_5) AND ORC GENERATOR

Month	Feb.	May	Aug.	Nov.
Solar irradiation (W/m²)	971.13	883.01	872.71	951.40
T_3 (°C)	201.38	191.85	189.93	201.27
T_5 (°C)	169.25	162.90	161.61	169.18
T_6 (°C)	72.88	76.05	76.69	72.91
\dot{m}_{ORC} (kg/s)	262.76	258.08	257.20	262.70
$Power_{net}$ (MW)	7.72	7.11	6.99	7.71
η_{ORC} (%)	12.38	11.76	11.63	12.37

OUTLET (INLET TO THE STORAGE TANK) (T_6) AND ORC PERFORMANCE RESULTS OBTAINED FOR FOUR DIFFERENT MONTHS AT TEZPUR, ASSAM WITH R245FA AS WORKING FLUID

The performance results shown in Table II are presented using R245fa as the working fluid in the ORC. R245fa

was selected based on evaluating ORC performance with five different working fluids. It was observed that using R245fa in the ORC produces the highest net power and efficiency. This is shown in Table III and these results of Table III correspond to the month of February. The mass flow rate of working fluid was highest for R245fa as a result of which maximum power was obtained in the ORC. This maximum power produced could be due to the thermodynamic properties of R245fa.

Table III
ORC PERFORMANCE RESULTS OBTAINED FOR FIVE DIFFERENT WORKING FLUIDS ALONG WITH THEIR CRITICAL PRESSURE AND TEMPERATURES (p_c and T_c) DURING FEBRUARY

Working fluid	T_c (°C)	p_c (kPa)	\dot{m}_{ORC} (kg/s)	$Power_{net}$ (MW)	η_{ORC} (%)
Iso-pentane	187.20	3378	131.80	7.22	12.78
R245ca	174.42	3925	241.55	7.56	12.54
Neo-pentane	160.59	3196	150.79	7.19	12.62
R245fa	154.01	3651	262.76	7.72	12.38
Butane	151.97	3796	134.92	7.57	12.52

The mass flow rate although it was not the least in case of neo-pentane, but the net power output of the ORC was minimum for neo-pentane. It may also be mentioned that this analysis was done with a constant 45°C of superheating, but actually the degree of superheating needs to be determined separately for the working fluids so that the ORC power output for a given working fluid is maximized. For the month of February, the difference in enthalpy between state points 2 and y for R245fa was 237.22 kJ/kg against an enthalpy difference of 377.86 kJ/kg corresponding to neo-pentane. On the other hand, the HTF temperature at ORC vapour generator exit was less for R245fa (72.88°C) compared to that of neo-pentane (72.91°C). Therefore with fixed 169.25°C HTF temperature at ORC vapour generator inlet (in February), amount of heat supplied was higher and more vapour (\dot{m}_{ORC}) could be generated with R245fa as working fluid in the ORC.

5. Conclusions

In this study, the thermodynamic analysis of a solar ORC based power is performed. The simulation is done for the geographical location of Tezpur, Assam and performance of solar based ORC system is evaluated for four different months viz. February, May, August and November. For the ORC, five different working fluids were considered and the highest net power was obtained with R245fa while the obtained net power was the

minimum for Neo-pentane for a given month. Thus, it is advisable to use R245fa in the ORC system operating in the considered geographical location to yield maximum power output.

References

- [1] Shabaan, S., 2016, Analysis of an integrated solar combined cycle with steam and organic Rankine cycles as bottoming cycles, *Energy Conversion and Management*, 126, pp. 1003-1012.
- [2] Helvacı, H.U. and Khan, Z.A., 2017, Thermodynamic modelling and analysis of a solar organic Rankine cycle employing thermofluids, *Energy Conversion and Management*, 138, pp. 493-510.
- [3] Al-Sulaiman, F.A., Dincer, I. and Hamdullahpur, F., 2011, Exergy modeling of a new solar driven trigeneration system, *Solar Energy*, 85, pp. 2228-2243.
- [4] Fernandez-Garcia, A., Zarza, E., Vazquez, L. and Perez, M., 2010, Parabolic-trough solar collectors and their applications, *Renewable Sustainable Energy Review*, 14, pp. 1695-1721.
- [5] He, C., Liu, C., Gao, H., Xie, H., et al., 2012, The optimal evaporation temperature and working fluids for subcritical organic Rankine cycle, *Energy*, 38, pp. 136-143.
- [6] Bellos, E. and Tzivanidis, C., 2018, Investigation of a hybrid ORC driven by waste heat and solar energy, *Energy Conversion and Management*, 156, pp. 427-439.
- [7] Boyaghchi, F.A. and Heidamejad, P., 2015, Thermoeconomic assessment and multi objective optimization of a solar micro CCHP based on Organic Rankine Cycle for domestic application. *Energy Conversion and Management*, 97, pp. 224-234.
- [8] Karellas, S., Leontaritis, A.D., Panousis, G., Bellos, E. and Kakaras, E., 2013, Energetic and exergetic analysis of waste heat recovery systems in the cement industry, *Energy*, 58, pp. 147-156.
- [9] Linke, P., Papadopoulos, A.I. and Seferlis, P., 2015, Systematic methods for working fluid selection and the design, integration and control of organic Rankine cycles – a review, *Energies*, 8, pp. 4755-4801.
- [10] Bao, J. and Zhao, L., 2013, A review of working fluid and expander selections for organic Rankine cycle, *Renewable Sustainable Energy Reviews*, 24, pp. 325-342.
- [11] Desai, N.B. and Bandyopadhyay, S., 2016, Thermoeconomic analysis and selection of working fluid for solar organic Rankine cycle, *Applied Thermal Engineering*, 95, pp. 471-481.
- [12] Maleki, S.A.M., Hizam, H. and Gomes, C., 2017, Estimation of Hourly, Daily and Monthly Global Solar Radiation on Inclined Surfaces: Models Re-Visited, *Energies*, 10(1), 134.
- [13] Forristal, R., 2003, Heat transfer analysis and modeling of a parabolic trough solar receiver implemented in Engineering Solver Equation, Technical Report No. NREL/TP-550-34169, U.S. National Renewable Energy Laboratory, Golden, Colorado 80401-3393.
- [14] Al-Sulaiman, F.A., 2014, Exergy analysis of parabolic trough solar collectors integrated with combined steam and organic Rankine cycles, *Energy Conversion and Management*, 77, pp. 441-449.
- [15] Bellos, E. and Tzivanidis, C., 2018, Investigation of a hybrid ORC driven by waste heat and solar energy, *Energy Conversion and Management*, 156, pp. 427-439.
- [16] Tzivanidis, C., Bellos, E. and Antonopoulos, K.A., 2016, Exergetic, energetic and financial evaluation of a solar driven absorption cooling system with various collector types, *Applied Thermal Engineering*, 102, pp. 749-759.
- [17] Tzivanidis, C., Bellos, E., Korres, D., Antonopoulos, K.A. and Mitsopoulos, G., 2015, Thermal and optical efficiency investigation of a parabolic trough collector, *Case Studies in Thermal Engineering*, 6, pp. 226-237.
- [18] Tzivanidis, C., Bellos, E. and Antonopoulos, K.A., 2016, Energetic and financial investigation of a stand-alone solar-thermal Organic Rankine Cycle power plant, *Energy Conversion and Management*, 126, pp. 421-33.

- [19] Lemmon, E.W., Huber, M.L. and McLinden, M.O., 2010, NIST Standard Reference Database 23: Reference Fluid Thermodynamic and Transport Properties-REFPROP 9.0, NIST.

Enhancement of Heat Transfer Rate in Sinusoidal Channel

Hirak Jyoti Kakati
hirak98765@gmail.com

Partha Pratim Dutta
ppdutta06@gmail.com

Pooja Dutta
poojadutta132@gmail.com

Abstract—Corrugations in plate heat exchangers enhances due high turbulence and improve the heat transfer rates up to 20–30% by increasing the heat transfer area. A two-dimensional heat transfer and fluid flow study was investigated for the sinusoidal corrugated duct. Taking air as the working fluid with a density of 1.225kg/m³ and inlet temperature 380K, the fluid was passed through the channel between the plates. Variations of Nusselt number, change of velocity and pressure drop along the arc length of the corrugated channel had been computed for the geometry. The commercial COMSOL Multiphysics software was used to study the flow features in a corrugated channel. A standard $k-\epsilon$ turbulence model coupled with heat transfer in fluids model were employed to account for turbulence and heat transfer in the flow. It was found that Nusselt number variation from the inlet to outlet is 49-65. Similarly, velocity variations and pressure drops are 2-2.35 m/s and 1.53 Pa.

Keywords: Heat Exchanger, Nusselt Number, Turbulent Flow, Heat Transfer, Corrugated.

1. Introduction

A heat exchanger is a mechanical device that is used to transfer thermal energy from higher to lower temperature fluid. In the recent years, the importance of the development of efficient heat exchangers has grown from the aspects of energy conservation, conversion, recovery, and successful implementation of new energy sources. Compact heat exchangers are characterized by high heat transfer coefficients compared to other exchanger types. Research has been done to obtain heat exchanger with high effectiveness, low-pressure losses, low weight and volume, high reliability and low cost. To obtain these requirements, heat exchanger contains special geometries like corrugation, wavy and curved flow channels to enhance the heat transfer rate. Both numerical and experimental studies are carried out to investigate the interaction between the flow behaviour within heat exchangers in order to optimize and design better units for specific applications.

2. Literature Review

Experiments on different corrugated configurations were carried out in the past. Mohammed et al. [1] made a study on the effects of geometrical parameters of a corrugated channel with out of phase arrangement. They studied the effects of corrugated tilt angles, channel heights, and wavy heights. The investigation covered Reynolds number and heat flux in the range 8000-20000 and 0.4-6 kW/m². It was reported that Nusselt number increased with the increase of wavy height. The numerical results indicated that the wavy angle of 60° and wavy height of 2.5 mm with channel

height of 17.5 mm were the optimum parameters. Tokzok et al. [2] made an investigation of flow characteristic and heat transfer enhancement. They studied the effects of aspect ratio on heat transfer enhancement. Aspect ratio reported to increase with heat transfer rate. Kim et al. [3] made an experimental study on corrugated cross-flow air-cooled plate heat exchangers. They tested single wave and doubled wave cross-flow air cooled plate heat exchanger(PHE) of 30-degree chevron angle. It was reported that doubled wave PHE showed higher cooling capacity due to the enhanced surface of doubled wave corrugation. Naphon [4] studied the effect of wavy plate geometry configurations on the temperature and flow distributions. A finite volume method with the structured uniform grid system was used to solve the turbulent model. Effects of geometry configuration of wavy plates, wavy plate arrangements, and air flow rates on the temperature and flow developments were considered. It was reported that the temperature gradients increased with increasing air flow rate. Gao et al. [5] made a numerical study on turbulent flow and heat transfer characteristics in cross-corrugated triangular ducts with delta-shaped baffles. The Re varied from 1000 to 6000. It was reported to find that 60° apex angle performs best in heat transfer when corrugation height was equal to baffles height and Nu increased by 2.1-4.3 times. Kiliç et al.[6] made an experimental investigation of heat transfer and effectiveness in corrugated plate heat exchangers having different chevron angles. The chevron angles are taken as 30° and 60°. It was reported to find that at 60° chevron angle we get higher heat transfer rate and effectiveness. Selvaraj et al. [7] made a numerical study of heat transfer analysis of different grooved geometries.

Based on computational fluid dynamics analysis the average Nusselt number was reported to increase up to 37%, 26%, and 42% for circular, square and trapezoidal grooved tubes, respectively, while compared with the plain tube. Yin et al. [8] made a numerical study of the effects of wavy plate phase shift on flow and heat transfer characteristics in the corrugated channel. It was reported to find that the friction factor and Nusselt number decreased with the increase of the phase shifts. Islamoglu et al. [9] made a study on the effect of channel height on the enhanced heat transfer characteristics in a corrugated heat exchanger channel. Here experiments were performed to determine forced convection heat transfer coefficients and friction factor for air flowing in corrugated channel employed in plate heat exchangers. Measurements were performed for two different values of channel height 5 and 10 mm for a single corrugation angle of 20° . The flow rate was varied over the range 1200 to 4000 Reynolds number. The Nusselt number and friction factor increased with the channel height. It was reported that the Nusselt number for the corrugated channel was higher than the straight channel. Nusselt number exceeded the straight channel value by 15% at $Re=1200$ and 75% at $Re=4000$ (At $H=5\text{mm}$). Again for channel height $H=10\text{mm}$, it was exceeded by 160% at $Re=1200$ and 250% at $Re=4000$. But the friction factor decreased with the Reynolds number. Pehlivan et al. [10] experimentally investigated the heat transfer rate for the sinusoidal corrugated channel. The experiment was carried out for constant heat flux of 616 W/m^2 , varied Reynolds number 1500 to 8000 for the corrugation angle 27° , 50° and 60° and channel height of 5 and 10 mm. It was reported that with an increased angle, the Nusselt number increases. The Nusselt number for $H = 5\text{ mm}$ was about 80% higher than for $H = 10\text{ mm}$ at $Re = 4000$, and the trend was that at a higher Reynolds number the Nusselt number was higher, reaching approximately 100% at $Re = 6000$. Abed et al. [11] studied on the enhancement of heat transfer in the channel with V-shaped wavy lower plate using liquid nanofluids. The computations were performed on uniform heat flux over a range of Reynolds number 8000–20,000. The governing equations were numerically solved in the domain by a finite volume method (FVM) using the $k-\epsilon$ standard turbulent model. Studies were carried out for different types of nanoparticles Al_2O_3 , CuO , SiO_2 and ZnO with different volume fractions in the range of 0–4%. Three different types of base fluid (water, glycerine, ethylene glycol) were also examined. It was reported to find that the average Nusselt number for nanofluids was greater than that of the base liquid. Heat transfer was found to increase with the increase in volumetric concentration but it was accompanied by increasing pressure drop. Moreover, the average Nusselt number increased with an increase in Reynolds number and volume concentration. Yang et al. [12] carried out an investigation on fluid flow and heat transfer characteristics in a channel with heated V corrugated

upper and lower plates. The parameters studied include the Reynolds number ($Re = 2,000\text{--}5,500$), angles of V corrugated plates (20 , 40 and 60) degrees, and constant heat fluxes ($q = 580, 830, 1,090\text{ W/m}^2$). Numerical results were validated using the experimental data reported by Naphon, and a good agreement was found. It was reported that with the increased of angles of V corrugated plates the heat transfer performance become better. Akdag et al. [13] numerically investigated heat transfer enhancement with nanofluids under laminar pulsating flow in a trapezoidal-corrugated channel. The results indicated a good potential in promoting the thermal performance enhancement by using the nanoparticles under pulsating flow. It was reported that the use of nanoparticles under the pulsating flow conditions increased the heat transfer rate.

Above mentioned is the overview of the different research works that have been contributed to the understanding of the performance of the corrugated heat exchangers. The present study has been undertaken to analyze the flow and heat transfer characteristics of a sinusoidal corrugated plate heat exchanger. Both numerical and experimental analysis has been carried out in the analysis

3. Methodology

Numerical analysis of results in COMSOL Multiphysics.

Steps involved in this CFD simulation are:

- Geometry modelling
- Mesh generation
- Defining physics and solution
- Post-processing

4. Boundary Conditions

In the present study, the boundary conditions imposed on the corrugated plate is wall boundary condition, while they are thermally insulated. The flow is assumed to be turbulent. Velocity boundary conditions are applied at the inlet while, pressure boundary conditions are applied at the outlet.

At the wall: $U=0, V=0$ where U and V are the velocities in the x and y directions.

At the inlet: $U=U_{in}, V=0$ and $T=T_{in}$

Where T_{in} is the temperature of the fluid at the inlet after a constant heat is given to the fluid.

At the outlet: the flow may safely be assumed as fully developed which implies negligible streamwise gradients of all variables.

5. Experimental Analysis

The effects of corrugations were studied experimentally. The variation of velocity, pressure drop and Nusselt number were studied along the arc length. Fig.1 represents an isometric view of experimental set up, Fig.2 and Fig.3 represent sinusoidal corrugated plate and Fig.4 represents detailed experimental setup with computer interface.

Components used in the setup:

1. Anemometer
2. K-type thermocouple
3. Speed variable air blower
4. Heater plate
5. Corrugated plate
6. Plain plate
7. Temperature data logging system

The length of the plate is 262.5 mm, width 150 mm, channel height 20 mm and corrugation height 10 mm. The fluid used in the analysis is air with a density of 1.225 kg/m^3 . The air with an inlet temperature of 380 K and inlet velocity 2 m/s is passed through the channel between the plates and in the process, it transfers heat to the plates which are at room temperature.

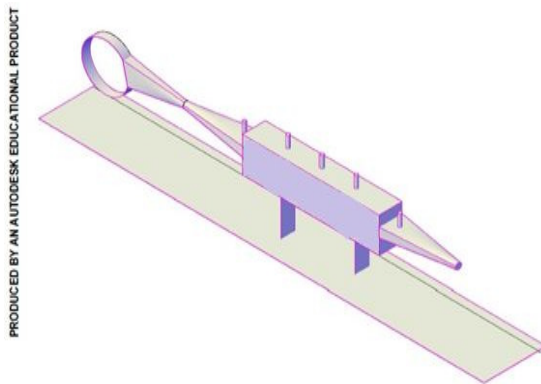


Fig.1 Isometric view of the experimental set up made in AutoCAD

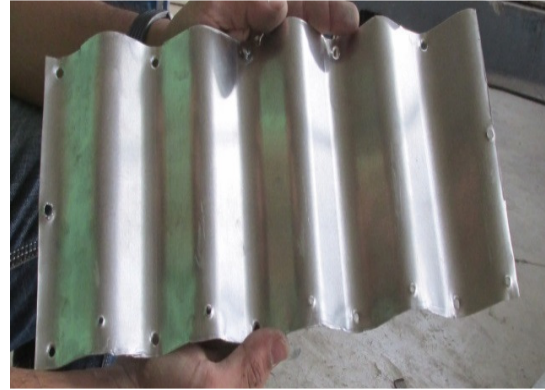


Fig.2 Sinusoidal Corrugated plate



Fig. 3 Test section for sinusoidal geometry



Fig.4 Experimental setup

6. Governing Equations

The governing equations are continuity, momentum and energy equation. The equations are given as:

$$\frac{\partial}{\partial x_i}(\rho u_i) = 0 \dots\dots\dots(1)$$

$$\frac{\partial}{\partial x_i}(\rho u_i T) = \frac{\partial}{\partial x_j}[(\Gamma + \Gamma_t) \frac{\partial T}{\partial x_j}] \dots\dots\dots(2)$$

$$\frac{\partial}{\partial x_i}(\rho u_i u_j) = -\frac{\partial p}{\partial x} + \frac{\partial}{\partial x_j}[\mu(\frac{\partial u_i}{\partial x_j} + \frac{\partial u_j}{\partial x_i})] + \frac{\partial}{\partial x_j}(-\rho \overline{u_i' u_j'}) \dots\dots\dots(3)$$

The last term of the momentum equation is called the Reynolds Stresses, τ_{ij} . Boussinesq hypothesis can be used to model the Reynolds stresses. The molecular thermal diffusivity and turbulent thermal diffusivity are defined as

$$\Gamma = \frac{\mu}{Pr} \text{ and } \Gamma_t = \frac{\mu_t}{Pr_t} \dots\dots\dots(4)$$

In the present study, the standard $k-\epsilon$ model is used. The standard $k-\epsilon$ model is a model based on model transport equations for the turbulence kinetic energy (k) and its dissipation rate (ϵ). The boundary conditions imposed on the corrugated plate are no slip and zero heat flux, while they are thermally insulated. The flow is assumed to be turbulent and incompressible. Velocity boundary conditions are applied at the inlet while, pressure boundary conditions are applied at the outlet.

The governing equations for the standard $k-\epsilon$ model are:

$$\frac{\partial}{\partial x_i}(\rho k u_i) = \frac{\partial}{\partial x_j}[(\mu + \frac{\mu_t}{\sigma_k}) \frac{\partial k}{\partial x_j}] + G_k - \rho \epsilon \dots\dots\dots(5)$$

$$\frac{\partial}{\partial x_i}(\rho \epsilon u_i) = \frac{\partial}{\partial x_j}[(\mu + \frac{\mu_t}{\sigma_\epsilon}) \frac{\partial \epsilon}{\partial x_j}] + C_{1\epsilon} \frac{\epsilon}{k} G_k - C_{2\epsilon} \rho \frac{\epsilon^2}{k} \dots\dots\dots(6)$$

Modelling the Turbulent Viscosity:

$$\mu_t = \rho C_\mu \frac{k^2}{\epsilon} \dots\dots\dots(7)$$

Here $G_k = -\rho \overline{u_i' u_j'} \frac{\partial u_j}{\partial x_i} \dots\dots\dots(8)$

Constants are

$$C_{1\epsilon} = 1.44, C_{2\epsilon} = 1.92, C_\mu = 0.09, \sigma_k = 1.0, \sigma_\epsilon = 1.3 \dots\dots\dots(9)$$

The values of the constants have been reported to determine from experiments for fundamental turbulent

flows including frequently encountered shear flows like boundary layers, mixing layers and jets as well as for decaying isotropic grid turbulence [3]. It has been found to work fairly well for a wide range of wall-bounded and free shear flows. Here G_k is the generation of turbulence kinetic energy, u' and v' are the streamwise and transverse velocity component in x and y-direction respectively and σ is diffusion Prandtl number.

7. Results and Discussion

In this present work, we analysed the flow and heat transfer in the sinusoidal plate which is shown in the figures below. The length of the plate is 262.5 mm, width 150 mm, channel height 20 mm and corrugation height 10 mm. COMSOL Multiphysics Software with standard ($k-\epsilon$) turbulence model was used to solve the problem. Second-order upwind scheme and structured uniform grid system are used to discretize the main governing equations. The fluid used in the analysis is air with a density of 1.225 kg/m³. The air with an inlet temperature of 380 K and inlet velocity 2 m/s is passed through the channel between the plates and in the process, it transfers heat to the plates which are at room temperature

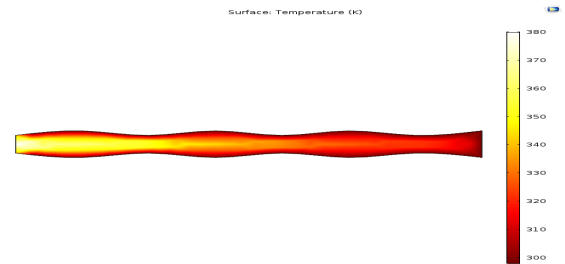


Fig. 5 Temperature profile for sinusoidal channel

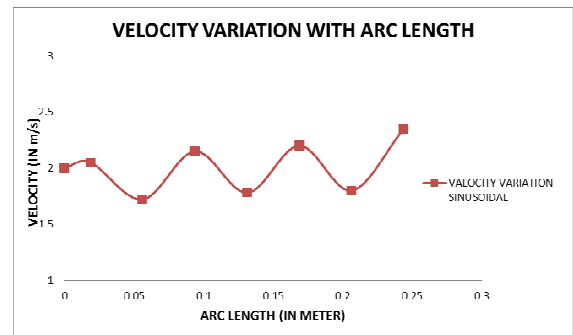


Fig. 6 Velocity profile for the sinusoidal channel

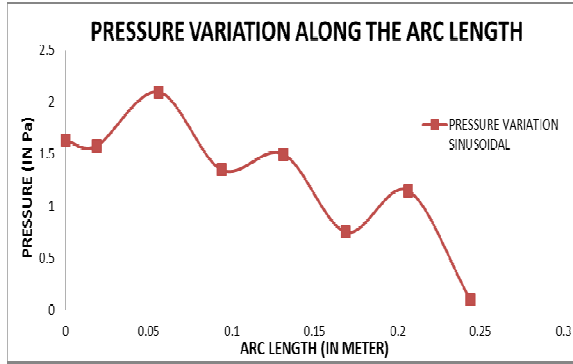


Fig.7 Pressure contour of sinusoidal channel

In fig. 5 temperature profile is shown. It was found that fluid temperature drops from the inlet to outlet. Here yellow colour showed a higher temperature than the red colour. In fig. 6 velocity profile is shown. It was found that fluid velocity increased in converging section than the diverging section. Here red colour showed higher velocities. From fig. 7 it was found that pressure drops along the arc length. Here red coloured lines showed the higher pressure. It was found that Nusselt number variation from the inlet to outlet is 49-65. Similarly, velocity variations and pressure drops are 2-2.35 m/s and 1.53 Pa. The Nusselt number was higher in the converging section of each wave than in the diverging section (furrow). This was because the converging section had a higher velocity gradient which increases the heat transfer ratio. Conversely, the flow had a low-velocity gradient near the wall surface in each furrow, which decreases the heat transfer ratio. The pressure drop decreases in the region with a minimum cross-section because in these regions the velocity of flow increases.

8. Validation of Result

To validate the results, the results obtained from the numerical results are compared with the experimental results.

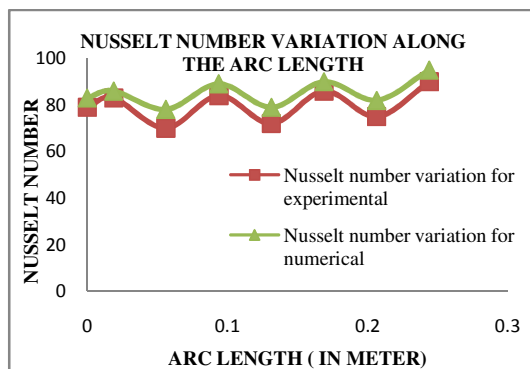


Fig.8 Nusselt number variation for sinusoidal plate

In Fig. 8, the results obtained for the sinusoidal plate is compared. It was found that 8.53% deviation between experimental and numerical results.

9. Conclusion

A two-dimensional heat transfer and fluid flow study was investigated for the sinusoidal corrugated duct. The fluid used in the analysis was air with a density of 1.225 kg/m^3 . The air with an inlet temperature of 380 K was passed through the channel between the plates. In the process, it transfers heat to the plates which are at room temperature. Variations of Nusselt number change of velocity and pressure drop along the arc length of the corrugated channel had been computed for the geometry. The Nusselt numbers had a higher value at the ridge and lower at the furrow. It was found that Nusselt number variation from the inlet to outlet is 49-65. Similarly, velocity variations and pressure drops are 2-2.35 m/s and 1.53 Pa. It was found that 8.53% deviation between experimental and numerical results.

Acknowledgement

I take the opportunity to express my gratitude to all those who rendered their valuable assistance in this paper. First and foremost I would like to thank my project supervisor and Head of the Department Dr. Partha Pratim Dutta, Associate Professor, Department of Mechanical Engineering, Tezpur University who has been very helpful with his insight and kind words of encouragement. I would like to extend my gratitude towards all the faculty members and technical staff of the Department of Mechanical Engineering, Tezpur University for their kind co-operation and encouragement. My special thanks to all my friends and well-wishers who have been motivating forces. Finally, I want to thank my beloved parents and my brother for their constant support and selfless love throughout my life.

References:

- [1] Mohammed, H.A., Azahar, A.M. and Wahid, A.M., 2013, The effects of geometrical parameters of a corrugated channel with in out-of-phase arrangement, *International Communications Heat and Mass Transfer*, 40, pp. 47-50.
- [2] Tokgoz, N., Aksoy, M. M. and Sahin, B., 2017 Investigation of flow characteristics and heat transfer enhancement of corrugated duct geometries, *Applied Thermal Engineering*, 118, pp. 518-530.
- [3] Kim, M., Baik, Y.J., Park, S.R., Ra, H.S. and Lim, H., 2010, Experimental study on corrugated cross-flow air-cooled plate heat exchangers, *Experimental Thermal and Fluid Science*, 34, pp. 1265-1272.
- [4] Naphon, P., 2009, Effect of wavy plate geometry configurations on the temperature and flow distributions, *International Communications in Heat and Mass Transfer*, 36, pp. 942-946.
- [5] Gao, Y. and Li, Z., 2017, Numerical study of turbulent flow and heat transfer in cross-corrugated triangular ducts with delta-shaped baffles, *International Journal of Heat and Mass Transfer*, 108, pp. 658-670.
- [6] Kılıç, B., Ipek, O., 2016, Experimental investigation of heat transfer and effectiveness in corrugated plate heat exchangers having different

- chevron angles, *International Journal of Heat and Mass Transfer*, 53, pp. 725-731.
- [7] Selvaraj, P., Sarangan, J. and Suresh, S., 2013, Computational fluid dynamics analysis on heat transfer and friction factor characteristics of a turbulent flow for internally grooved tubes, *Thermal Science*, 17, pp.1125-1137.
- [8] Yin, J., Yang, G. and Li, Y., 2012, The effects of wavy plate phase shift on flow and heat transfer characteristics in corrugated channel, *Energy Procedia*, 14, pp.1566-1573.
- [9] Islamoglu, Y. and Parmaksizoglu, C., 2003, The effect of channel height on the enhanced heat transfer characteristics in a corrugated heat exchanger channel, *Applied Thermal Engineering*, 23, pp. 979-987.
- [10] Pehlivan, H., Taymaz, I. and Islamoğlu, Y., 2013, Experimental study of forced convective heat transfer in a different arranged corrugated channel, *International Communications in Heat and Mass Transfer*, 46, pp.106-111.
- [11] Abed, A.M., Sopian, K., Mohammed, H.A., Alghoul, M.A., Ruslan, M.H., Mat, S. and Al-Shamani, A.N., 2015, Enhance heat transfer in the channel with V-shaped wavy lower plate using liquid nanofluids, *Case Studies in Thermal Engineering*, 6, pp. 13-23.
- [12] Yang, Y.T. and Chen, P.J., Numerical simulation of fluid flow and heat transfer characteristics in channel with V corrugated plates, *Int. J. Heat Mass Transfer*, 46, pp. 437-445.
- [13] Akdag, U., Akcay, S. and Demiral, D., 2017, Heat transfer enhancement with nanofluids under laminar pulsating flow in a trapezoidal-corrugated channel. *Progress in Computational Fluid Dynamics*, An International Journal, 17, pp. 302-312.

Performance Analysis of a Coal Fired Open Cycle MHD Generator

Abhinav Dutta

abhinavdutta197@gmail.com

Jyantrik Dominoo Borah

dominoo.jyantrik@gmail.com

Ujjal Kumar Sen

ujjalkumarsen10110@gmail.com

Abstract— In the present work, a coal fired open cycle MHD generator's performance is analyzed with three different nozzles of different Mach numbers. Some standard equations are used to obtain the analytical solutions and the results are validated using finite element simulation in ANSYS. Disc MHD Generator is used for power generation.

Keywords— Electrical Energy, Thermal Plant, MHD Conversion System, Coal. Heat Energy

1. Introduction

Electrical energy is the most essential part of human life. We can use electrical energy to do any kind of machinery work. It can be converted to almost all kinds of energy available, besides it is renewable so it has more demand than the fossil energy. For decades people are trying to discover different methods for the generation of electrical energy efficiently. Our main source of energy is the sun and from that we are converting energy into different forms, electrical energy is mainly extracted from mechanical, solar and chemical energy. Today major part of the electrical energy is generated with the help of Faraday's law, here mechanical energy is converted to electrical energy. But Lenz law also can be used to convert mechanical energy into electrical energy and the method that is used to generate electrical energy with the help of Lenz law is called Magneto-hydrodynamics or MHD.

When an electric ion travels in a magnetic field it experiences a force along the direction which is perpendicular to both the magnetic field as well as the direction of the velocity of the ion. When an ionized gas or liquid passes through a magnetic field an EMF is generated perpendicular to the direction of the flow of the fluid and the magnetic field. Amount of EMF generated per unit area of the generator is equal to the product of the magnitude of the magnetic field and magnitude of velocity of the flow at the cross section where EMF will be generated. In this method kinetic energy of the fluid is converted to electric energy, according to Lenz law the flow of the fluid will be restricted by the induced magnetic field that will be formed by the newly formed electric field, so to produce and maintain the flow pressure energy is used and the pressure energy comes from the heat energy that is obtained by burning the fuel. Here we are using coal as the fuel.

2. Literature Review

There has been much ongoing research in the field of Electric power generation keeping in mind the tremendous need of electrical energy in every field of modern society. Since a decade the demand for electricity is increasing at alarming rate and the demand for power is running ahead of supply. The present day generation methods are not very

has forced the world to rethink & develop the Magneto Hydro Dynamic (MHD) type power generation which remained unthinkable for several years after its discovery. It is a unique and highly efficient method of power generation with nearly zero pollution. In advanced countries this technique is already in use but in developing countries it's still under construction.

A study was performed a study on the future prospects of MHD Generation. Efficiency matters the most for establishing a power plant. MHD power plants have an overall efficiency of 50-60% but it can be boosted up to 80% or more by using superconducting magnets in this process. Whereas the other non conventional methods of power generation such as solar, wind, geo-thermal, tidal have a highest efficiency not more than 35%. Hence by using MHD power generation method separately or by combined operation with thermal or nuclear plants we hope to bring down the energy crisis at a high rate. [1]

A study on Magnetohydrodynamic Generation. In this device plasma (Ionized gas) is the working fluid similar to the mechanism that happening in the magnetosphere of our earth's atmosphere. Except here the process is controlled and we increase the fluid density and pressure to get maximum efficiency in the generating power. Most problems come from the low conductivity feature in the gas at high temperature. High temperature gaseous conductor at high velocity is passed through a powerful magnetic field. [2]

A study was carried out an study on Conceptual Design Analysis of An MHD Power Conversion System for Droplet-Vapor Core Reactors, Innovative Nuclear space Power and Propulsion Institute University of Florida Gainesville, Florida. This report was prepared as an account of work sponsored by an agency of the United States Government. The objective of this project work is to develop a computer model to perform design analysis and study electrodynamic of linear MHD generator for the proposed space tower system. [3]

A study was performed analysis on Analysis and Performance calculation of 2MWe MHD Power Generators (KDF2-7). The performance calculation and

design feature of MHD generator KDF2-7 made by IEE (China) is presented. The generator can be configured electrically for either Faraday or the diagonal electrical mode through external electrical connections. Operating conditions and performance characteristics of both Faraday and diagonal channel including different diagonal angles were compared. Selecting some of the diagonal angles the power output of the diagonal channel can be closed to Faraday mode at same operating conditions. The performances diagrams in the dimensionless current density plan are presented and comparisons of both above generators are conducted. [4]

A study carried out an analysis of 120 MW thermal power plant with combined effect of constant inlet pressure (124.61 bar) and different inlet temperatures. In this paper, the thermodynamic analysis of 120 MW thermal power plant has been done at particular inlet pressure (124.61 bar) and at different inlet temperatures (507.78° C, 517.78° C, 527.78° C, 537.78° C, 547.78° C, 557.78° C, and 567.78° C). The correction curves for power and heat rate have been generated for combined effect of inlet pressure and different inlet temperatures. These curves indicate that if inlet pressure is 124.61 bar and inlet temperatures vary, then power output and heat rate also vary. [5]

An analysis of Integrated Systems based on MHD Generators. In this paper two plant configurations based on open-cycle MHD generators fed with coal are presented. The first one is a conventional configuration in which the plasma gas is the products of direct combustion of coal. The second one can be considered an advanced type because the working fluid is the combustion exhausts of syngas generated from coal gasification. In order to evaluate the energy suitability of the proposed systems, a performance analysis has been carried out by means of numerical modeling. Therefore, the operating conditions and the plant configurations for an efficient recovery of the thermal energy available from the MHD exhausts have been defined by a sensitivity analysis carried out varying the preheating temperature of air (or enriched air) sent to the combustion chamber. [6]

An analysis was performed on enhancement of Power Generation in Thermal Power Plant using MHD system. To fulfil the deficiency of electrical energy further enhancement of power plants is taking place, thereby causing severe air pollution. Present investigation deals with the enhancement of power generation in the existing power plants by incorporating the MHD system and also which reduces the air pollution problem. [7]

Energy harvesting is among a method that can contribute on the renewable energy. MHD power generator is a new way to harvest the energy especially Ocean wave energy. An experimental investigation was conducted to explore performance of MHD generator. The effect of intensity of NaCl solution (Sea water), flow rate of NaCl solution, magnetic strength and magnet position to the current produced was analyzed. The result gives that the individual factors had a significant effect to the current produced, because of that each factor need to be

considered on develop of MHD generator to harvest the wave energy as the alternative way to support the demand for energy. [8]

An analysis was carried out where the various concepts of MHD power generation are presented. The first one is zero stack emission power plants where some plants are proposed to drastically reduce the greenhouse gas emission. Preliminary studies have indicated that MHD/Steam plants have the highest efficiency when compared with other plants. Second one is aerospace applications of MHD generation. Plasma MHD generators fed by liquid or solid fuels has been proposed. An electrical power generation on board system was considered. [9]

A study was carried out to study the MHD technology including principle of operation, types, power extraction method. This paper also discusses the developments taking place in MHD power generation. [10]

An analysis of thermal efficiency of a magnetohydrodynamic (MHD) power cycle at maximum power density for a constant velocity type MHD Generators has been carried out. The irreversibilities at the compressor and the MHD generator are taken into account. The results obtained from power density analysis were compared with those of maximum power analysis. It is shown that by using the power density criteria the MHD cycle efficiency can be increased effectively. [11]

A mathematical modeling of MHD processes has been done then experimental results obtained through prototype model verified with simulated results using MATLAB. The MHD generator prototype that is developed and discussed in this research paper is closed cycle. MHD close cycle has been used for less consumption of electrolyte and due to cost effectiveness. The voltage induced in this prototype is 2-3V that can be improved by scaling some parameters (Magnetic field effect, velocity of fluid, selection of materials and solution) carefully. [12]

A discussion is given of the basic physical processes occurring in MHD generators. In designing a generator two parameters are of importance, namely, the power output per unit volume and the isentropic efficiency which is a measure of departure of the generation processes from the ideal. The paper discusses how the isentropic efficiency depends on the load characteristics, how to calculate the electrical conductivity, the effect of strong magnetic field on the electrical conductivity and optimum shape of an MHD duct. A brief account is given of the progress in the development of experimental generators and of the practical problems still to be solved. [13]

A study includes estimated cost data for MHD as well as known cost data for existing power production methods. Data was also researched to compare MHD environmental effects with those of other power generation methods. The research methodology involves analyzing tests, special

reports on MHD, power production cost data, transmission studies, periodical literature, hearings and conferences on MHD, statements, reports, power consumption data, power production forecasts, personal interviews and correspondence. [14]

The various nozzle flow characteristics and the equations for a convergent-divergent nozzle was studied and taken from the textbook Introduction to Fluid Mechanics and Fluid Machines. [15]

3. Objectives

The objectives of this project are :-

(1) Performance analysis of a coal fired open cycle MHD plant at different Mach numbers of Nozzle

(2) To analyze the variations of pressure, temperature, Mach number and velocity of the combustible gas along the length of the convergent-divergent nozzle.

4. Open Cycle MHD

The MHD generator is similar to that of rocket engine except surrounded by a magnet that is to produce external magnetic field. Once the gas is heated to 2750 to 3000 K and pressurized to 7 to 15 bar pressure a small fraction ionized alkali metal like cesium or potassium is injected to increase the electric conductivities of gas. While expanding in the presence of powerful magnet, the positive and negative ions move to the electrodes and constitute an electric current. This is basically Faraday's law of motional electromagnetic induction. But not the usual one, in which charge flows in a conductor when time varying magnetic field is applied. Here both electrons and heavy gas particles are in thermal equilibrium due to high collision frequencies and energy transfer/collision.

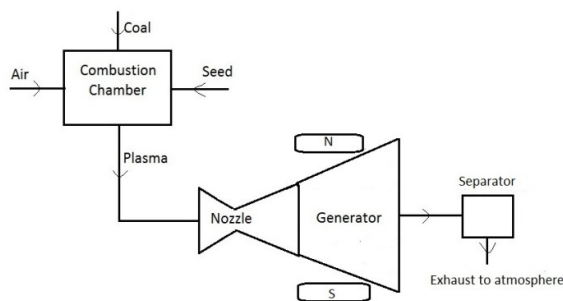


Fig 1: Layout diagram of an open cycle MHD cycle

4.1 Process Description

At first air goes to the Combustion Chamber and it is burned with coal and seed material is added to it. Seed materials are added to enhance the ionization capacity of the flow gas. Then the high pressure flow gas goes through a converging-diverging nozzles of the MHD generator where the potential energy is converted to kinetic energy and the flow gas gets a very high velocity. The high velocity flow gas passes through a Disc MHD generator where a strong magnetic field is applied transversely and

according to Lenz law an EMF is generated across the generator. The exhaust gas passes through a separator and the seed materials are removed from the flow gas, before the gas is released to the atmosphere.

5. Coal Selection and Specifications

Coal is used as fuel in the MHD cycles, Coal contains variable amounts of carbon, Hydrogen, Nitrogen, Sulphur and other impurities. Coal is directly inserted in the combustion chamber where it is burnt to extract heat energy for the cycle

5.1 Types of coal in India

Depending upon its grade from highest to lowest following, The coal found in India can be classified as Anthracite Coal, Bituminous Coal, Lignite (Brown Coal), Peat etc. They are discussed below:-

5.1.1 Anthracite Coal

This is the best quality of coal and contains over 85 percent carbon. It is very hard, compact, jet black coal having semi-metallic lustre.

Anthracite coal ignites slowly and burns with a nice short blue flame. In India, it is found only in Jammu and Kashmir and that too in small quantity.

5.1.2 Bituminous Coal

This is the most widely used coal and contains 50 to 85 percent carbon. It is dense, compact, and brittle and is usually of black colour.

A good bituminous coal is composed of alternate dull and bright bands. Its calorific value is very high due to high proportion of carbon and low moisture content. Most of the bituminous coal is found in Jharkhand, Orissa, West Bengal, Chhattisgarh and Madhya Pradesh.

5.1.3 Lignite or Brown Coal

This is also known as brown coal, lignite is a lower grade coal and contains about 35-50 per cent carbon. It represents the intermediate stage in the alternation of woody matter into coal. Its colour varies from dark to black brown. It is found in Palna of Rajasthan, Neveli to Tamil Nadu, Lakhimpur of Assam and Karewa of Jammu and Kashmir.

5.1.4 Peat

This is the first stage of transformation of wood into coal and contains less than 35 per cent carbon. It is seldom sufficiently compact to make a good fuel without compressing into bricks. Left to itself, it burns like wood, gives less heat, emits more smoke and leaves a lot of ash after burning.

After analysing the properties of different coal that are available in India we have decided to use the Bituminous coal as fuel in our cycles. Since Bituminous coal has the second highest carbon content, it is easily available in India and its cost is not so high.

5.2 Coal Analysis

Table 1: Proximate analysis

Constituents	Amount in %
Moisture (%)	5.18
Ash (%)	43.25
Volatile matter (%)	19.33
Fixed carbon (%)	32.24

Table 2: Ultimate analysis

Constituents	Amount in %
Moisture (%)	5.18
Mineral matter (%)	11.78
Carbon (%)	70.15
Hydrogen (%)	2.70
Nitrogen (%)	1.15
Sulphur (%)	0.47
Oxygen (%)	8.57

5.3 Heating Value of Coal

The heating value (or energy value or calorific value) of a substance, usually a fuel is the amount of heat released during the combustion of a specified amount of it. There are two types of heating values that are:

- High Heating Value (HHV)
- Low Heating Value (LHV)

5.3.1 High Heating Value (HHV)

The quantity known as higher heating value (HHV) (or gross energy or upper heating value or gross calorific value (GCV) or higher calorific value (HCV)) is determined by bringing all the products of combustion back to the original pre-combustion temperature, and in particular condensing any vapor produced. HHV calculation assumes that all of the water in a combustion process is in a liquid state after a combustion process.

5.3.2 Low Heating Value (LHV)

The quantity known as lower heating value (LHV) (net calorific value (NCV) or lower calorific value (LCV)) is determined by subtracting the heat of vaporization of the water from the higher heating value. LHV calculation assumes that the water component of a combustion process is in vapor state at the end of combustion.

From the above definitions we decided to take the HHV value as the heating value of our fuel.

Now we will determine the High Heating Value (HHV) of Bituminous coal

We are taking Dulong Formula for the calculation of HHV value for Bituminous Coal

$$\text{HHV} = 339C + 1427\left(H - \frac{O}{8}\right) + 225S \text{ KJ/kg} \text{ -----(1)}$$

Here, C : Carbon content in percentage in the coal

H : Hydrogen content in percentage in the coal

O : Oxygen content in percentage in the coal

S : Sulphur content in percentage in the coal

For Bituminous coal, C ≈ 70%

$$H \approx 4\%$$

$$O \approx 3\%$$

$$S \approx 3\%$$

$$\text{Ash} \approx 20\%$$

Now after inserting these values in equation (5.1) we have got that the HHV for Bituminous coal is approximately 6973.82 KCal/Kg or 29191.02 KJ/kg.

6. Calculations for Flow Rates and Adiabatic Flame Temperature

6.1 Mass Flow Rates

The balanced equation of Combustion of Coal is:
 $C + 2H_2 + N_2 + 2S + 3O_2 + (O_2 + 3.76N_2) \rightarrow CO_2 + 2H_2O + (4.76)N_2 + 2SO_2$

From stoichiometric calculations and percentage of chemical components present in the coal mass flow rate of air and fuel are found. The fuel flow rate is found to be 0.8 kg/Sec.

Stoichiometric Air-Fuel ratio: - 10:1

Considering 20% excess air during combustion, the actual Air-Fuel ratio is: - 12:1

Therefore, Mass Flow Rate of Air, $m_{\text{air}} = 9.5 \text{ kg/Sec.}$

Therefore, Mass Flow Rate of Gas, $m_{\text{mixture}} = m_{\text{air}} + m_{\text{fuel}}$
 $m_{\text{mixture}} = 10.3 \text{ kg/Sec.}$

Now, Mass Flow Rate of Seed, $m_{\text{seed}} = 1\%$ of m_{mixture}
 $m_{\text{seed}} = 0.103 \text{ kg/Sec.}$

So, Mass Flow Rate of Plasma, $m_{\text{plasma}} = m_{\text{mixture}} + m_{\text{seed}}$
 $m_{\text{plasma}} = 10.403 \text{ kg/Sec.}$

6.2 Adiabatic Flame Temperature

Adiabatic Flame Temperature is the maximum temperature that can be obtained from burning the fuel. After the reaction among the reactants the energy released gets divided into two parts some energy is used to form the products and the rest increases the temperature of the products. The energy released from the reactants is equal to the summation of enthalpy of formation of the reactants, similarly the energy used for the formation of the products is equal to the summation of enthalpy of formation of the products. And the energy used to increase the temperature of the products is equal to the summation of products of the specific heats and the temperature change of the products. Here we are taking the standard ambient

temperature 298 K as the initial temperature of the products. We will use the standard relation among the enthalpy of formation of reactants and products, specific heats of products and adiabatic temperature to find the adiabatic temperature of the reaction.

Therefore, $\Sigma H_R = \Sigma H_P + \Sigma C_P (T_{adia} - 298)$ ----- (2)

Where, H_R = Enthalpy of Formation of Reactants.
 H_P = Enthalpy of Formation of Products.
 C_P = Specific Heat of Products at Constant Pressure.
 T_{adia} = Adiabatic Flame Temperature.

The elements for which the values of H_R , H_P , and C_P are calculated are cited in the table given below.

Table 3: Enthalpy of formation and specific heat values

Reactants		Products		
Elements	H_R (KJ/mol)	Elements	H_P (KJ/mol)	C_P (KJ/mol-K)
C	0	CO ₂	-393.5	0.051
H ₂	0	H ₂ O	-281.8	0.012
N ₂	0	N ₂	0.0	0.032
O ₂	0	SO ₂	-332.9	0.041
S	0			

From equation (6.2) we have found that $T_{adia} = 7500$ K.

7. Nozzle Parameters

Nozzle is used to convert the potential energy of the plasma gas to kinetic energy, so that it moves through the MHD Generator with a very high velocity. Here we have considered three supersonic nozzles with different dimensions and parameters, after that we will compare the nozzle parameters of the three different nozzles and take the best nozzle for use in our cycle.

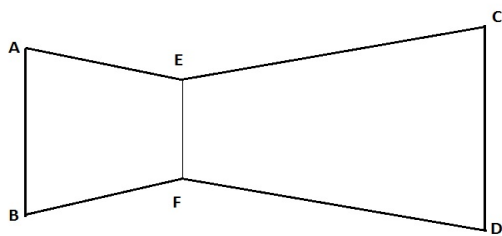


Fig 2: Converging-Diverging Nozzle

Here, AB is the Inlet diameter of the nozzle.
 CD is the Outlet diameter of the nozzle.
 EF is the Throat diameter of the nozzle.

The following parameters will be constant for all the three nozzles

- Distance between the Inlet to the Throat is 0.3 meter.
- Distance between the Throat to the Outlet is 0.7 meter.

- Total Length of the nozzle is 1 meter.
- Inlet and Throat diameters of the nozzle are 0.2 meter and 0.15 meter respectively.

7.1 Nozzle Equations

We have, $(\frac{A_i}{A^*})^2 = \frac{1}{M_i} [\frac{2}{(Y+1)} \{ 1 + \frac{(Y-1)}{2} M_i^2 \}]^{\frac{Y+1}{Y-1}}$ ----- (3)

Here, M_i is the Mach number at the inlet of the nozzle, A^* is the throat area of the nozzle, and A_i is the area of the inlet of the nozzle.

We have, $\frac{A_e}{A^*} = (\frac{Y+1}{2})^{\frac{-(Y+1)}{2(Y-1)}} \times \frac{(1 + \frac{Y-1}{2} M_e^2)^{\frac{Y+1}{2(Y-1)}}}{M_e}$ ----- (4)

Here, A_e is the outlet area of the nozzle, Y is the adiabatic gas constant and M_e is the Mach number of the nozzle. This equation will be used to calculate the M_e .

We have, $\frac{T_e}{T_i} = (1 + \frac{Y-1}{2} M_e^2)^{-1}$ ----- (5)

Here, T_e is the exit temperature of the nozzle, T_i is the inlet temperature of the nozzle. This equation will be used to calculate the outlet temperature of the nozzle.

We have, $\frac{T_{ad}}{T_i} = 1 + \frac{Y-1}{2} M_i^2$ ----- (6)

Here, T_{ad} is the adiabatic flame temperature, T_i is the temperature at the inlet of the nozzle.

We have, $P_t = \frac{m_{pl} \times \sqrt{T_i}}{A^* \times M_e \times \sqrt{\frac{Y}{R} (1 + \frac{Y-1}{2} M_e^2)^{\frac{1+Y}{1-Y}}}}$ ----- (7)

Here, P_t is the stagnation pressure of the nozzle, m_{pl} is the mass flow rate of the plasma, T_i is the adiabatic flame temperature of the nozzle, R is the Gas constant of plasma.

We have, $\frac{P_e}{P_t} = (1 + \frac{Y-1}{2} M_e^2)^{\frac{-Y}{Y-1}}$ ----- (8)

Here, P_e is the exit pressure of the nozzle.

We have, $C = \sqrt{YRT_e}$ ----- (9)

Here, C is the speed of sound at T_e (in °C) temperature.

We have, $U_e = M_e \times C$ ----- (10)

Here, U_e is the exit velocity of plasma in the nozzle.

We have, $U_i = M_i \sqrt{YRT_i}$ ----- (11)

Here, U_i is the velocity at the inlet of the nozzle.

Alternate equation, $U_e = \sqrt{2\eta_n (h_{oi} - h_{es})} \sqrt{2\eta_n C_P (T_{oi} - T_{es})}$ ----- (12)

Where η_n is the efficiency of the nozzle, h_{oi} is the stagnation enthalpy at the inlet of the nozzle, h_{es} is the enthalpy at the exit of the nozzle, T_{oi} is the stagnation temperature at the inlet of the nozzle, T_{es} is the temperature at the exit of the nozzle and C_p is the specific heat at constant pressure.

$$\text{We have, } \left(\frac{P_t}{P_i}\right) = \left(\frac{T_{ad}}{T_i}\right)^{\frac{\gamma}{\gamma-1}} \dots \dots \dots (13)$$

Where P_t is the stagnation pressure and P_i is the pressure at the inlet of the nozzle.

7.2 Nozzle Parameter Values

We have considered the inlet temperature for all the nozzles as 7500K and exit diameters of the nozzles as 0.25m, 0.30m and 0.35m respectively. After calculating the other parameters by putting these values in the above equations we got the values of the parameters as cited in Table 4 and Table 5.

Table 4: Nozzle Parameter values

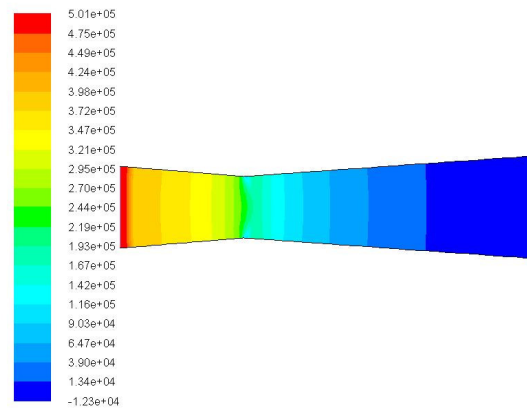
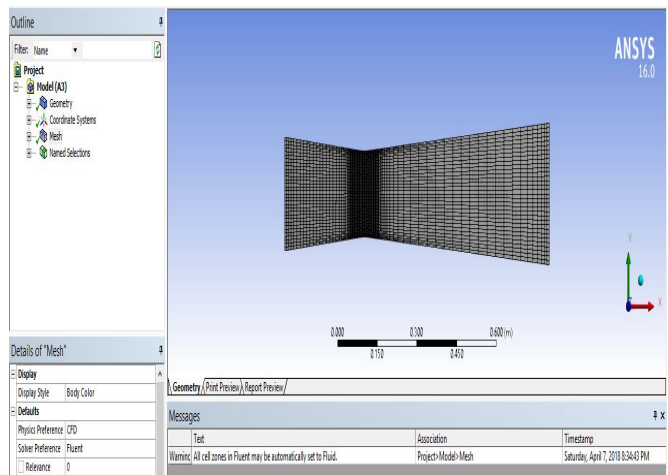
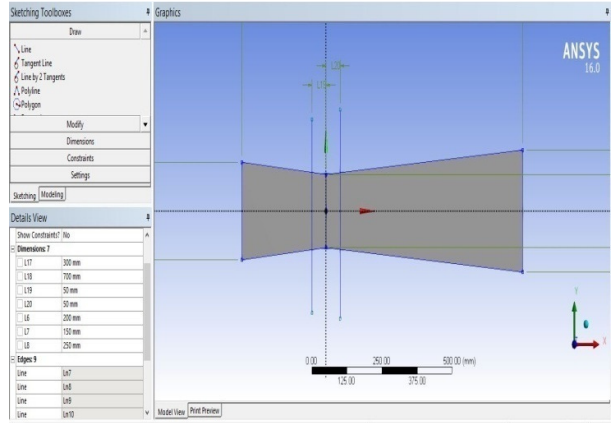
	M_i	M_e	$T_i(K)$	$T_e(K)$	P_t (bar)	P_i bar	P_e bar	U_e (m/s)	η_n in %
Nozzle 1	.6	2.2	2964.4	2702.7	4.38	3.2	.29	947.6	63.4
Nozzle 2	.6	2.5	2964.4	2635.0	4.38	3.2	.15	1063.2	65.06
Nozzle 3	.6	2.6	2964.4	2611.3	4.38	3.2	.12	1100.8	65.5

Table 5: Ansys parameter values

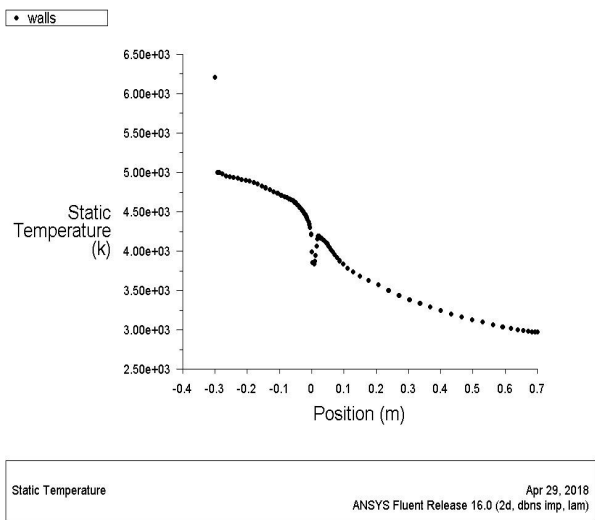
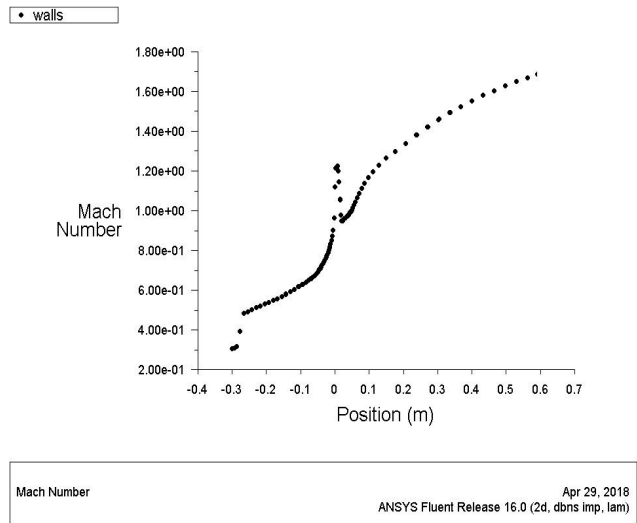
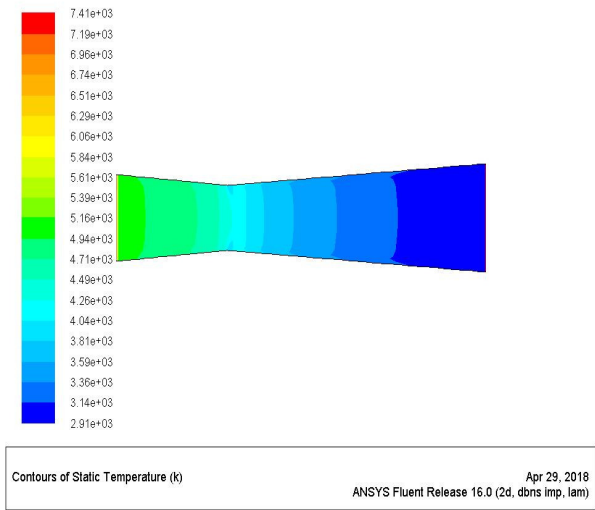
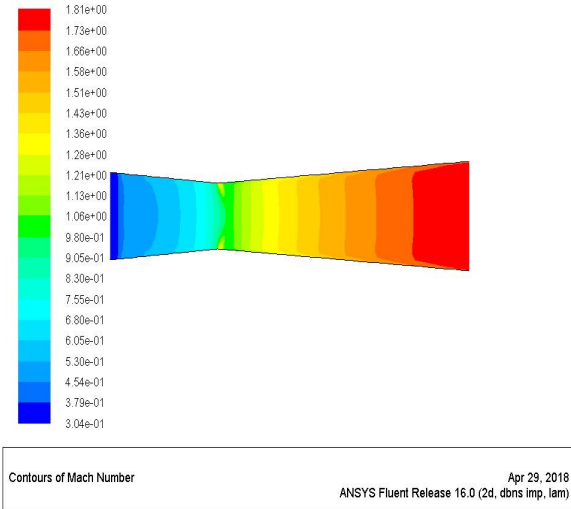
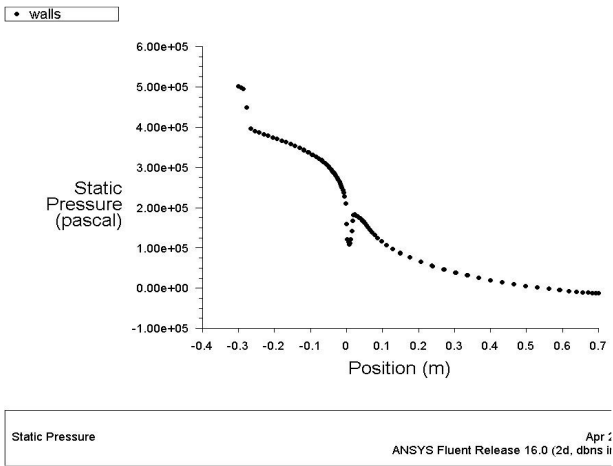
Parameters obtained from Ansys (while doing nozzle analysis)	Corresponding values (obtained)
Thermal Conductivity (k)	0.4 W/ m-K
Density of the plasma gas (ρ)	0.77 kg/m ³
Specific Heat (C_p)	238 J/kg-K
Gas Constant (R)	66 J/kg-K
Adiabatic Gas Coefficient (γ)	1.04

8. Nozzle Ansys Results

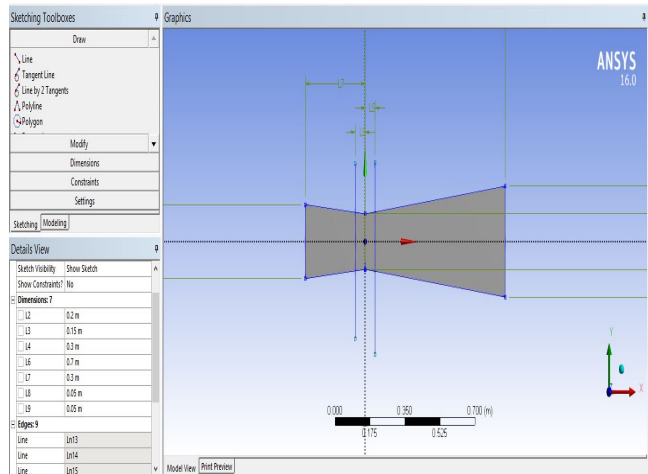
8.1 Nozzle 1

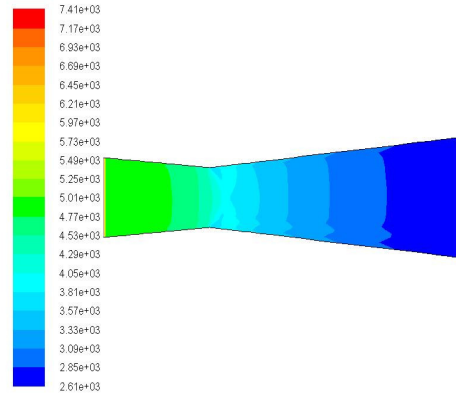
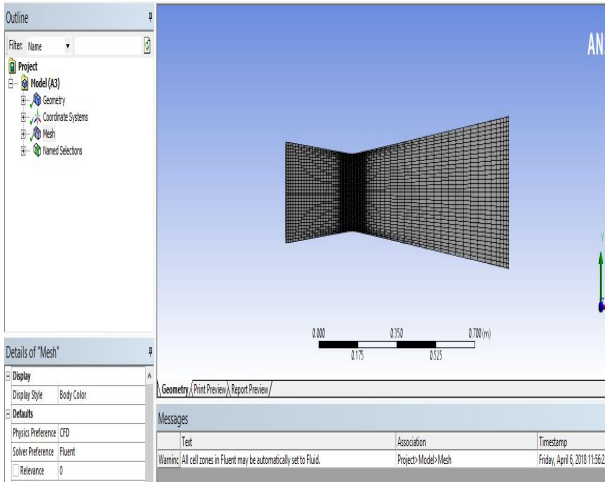


Contours of Static Pressure (pascal) ANSYS Fluent Release 16.0 (2d, dbrns imp. lam) Apr 29, 2018

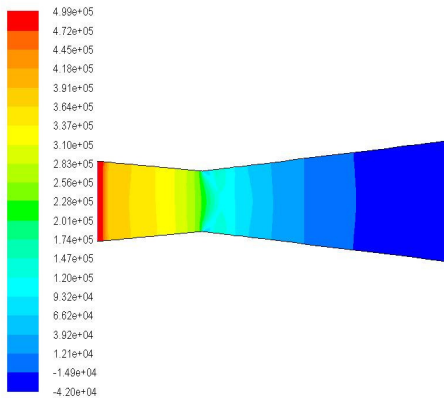


8.2 Nozzle 2

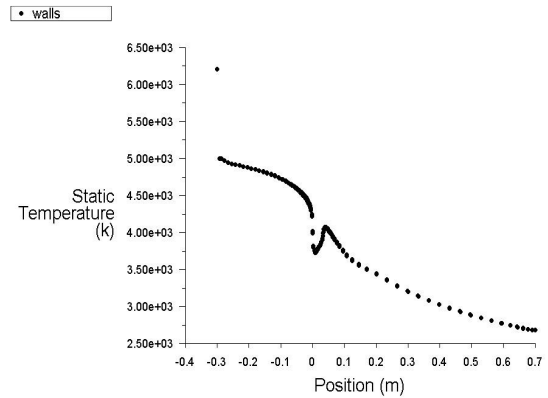




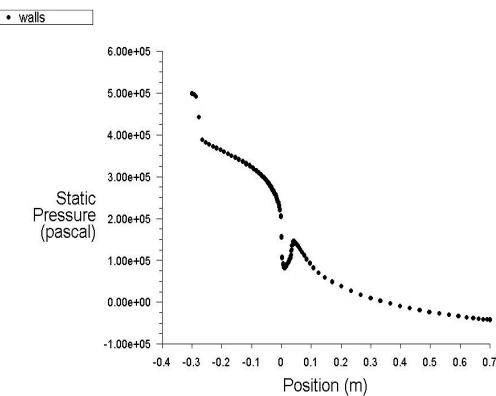
Contours of Static Temperature (k) Apr 29, 2018
ANSYS Fluent Release 16.0 (2d, dbns imp, lam)



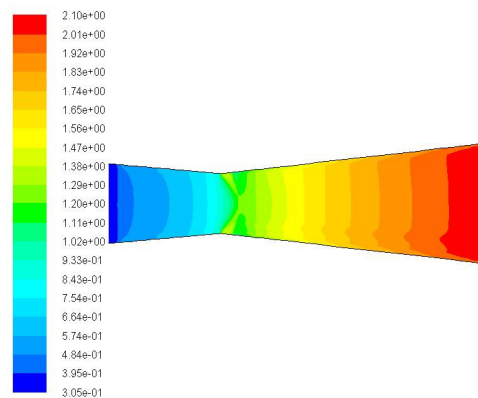
Contours of Static Pressure (pascal) Apr 29, 2018
ANSYS Fluent Release 16.0 (2d, dbns imp, lam)



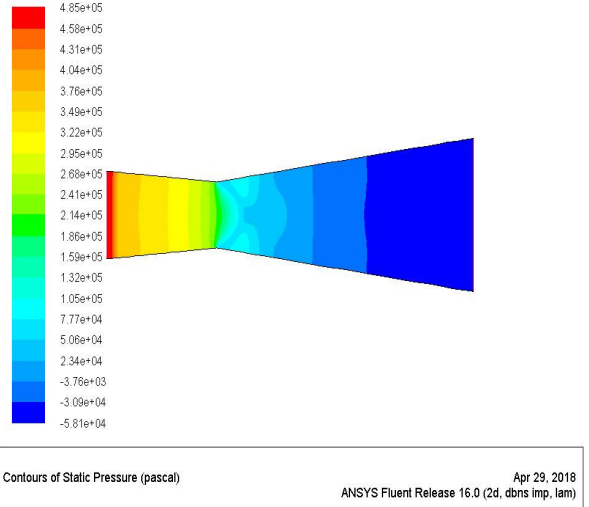
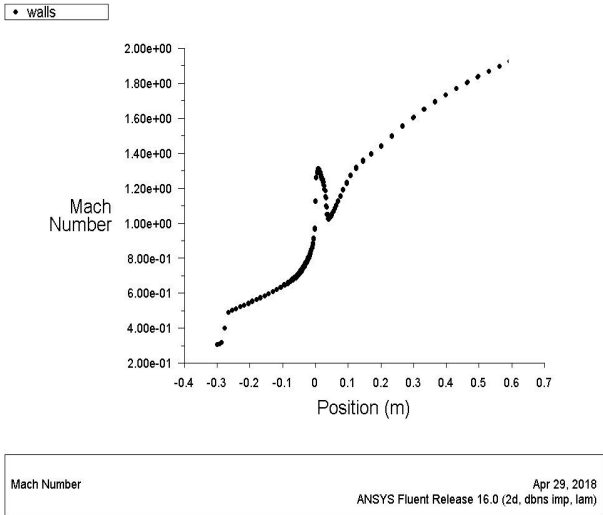
Static Temperature Apr 29, 2018
ANSYS Fluent Release 16.0 (2d, dbns imp, lam)



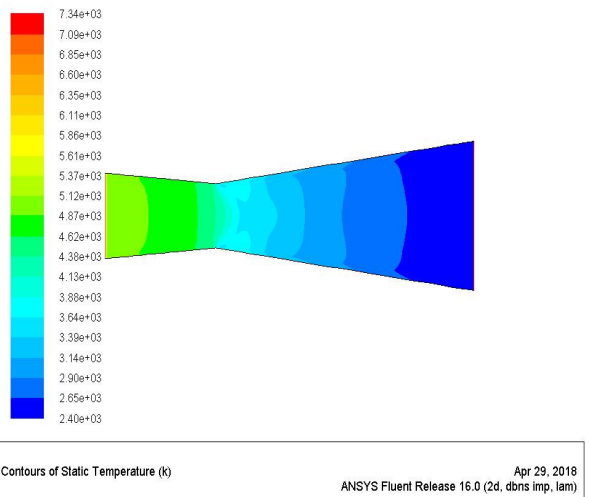
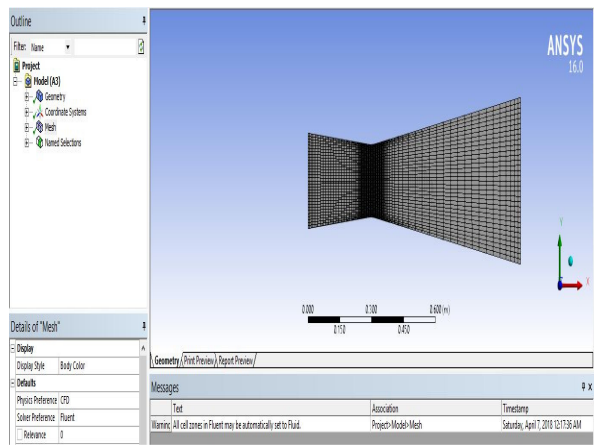
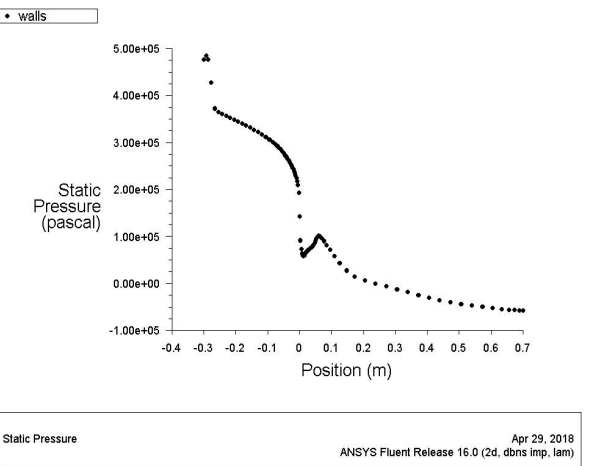
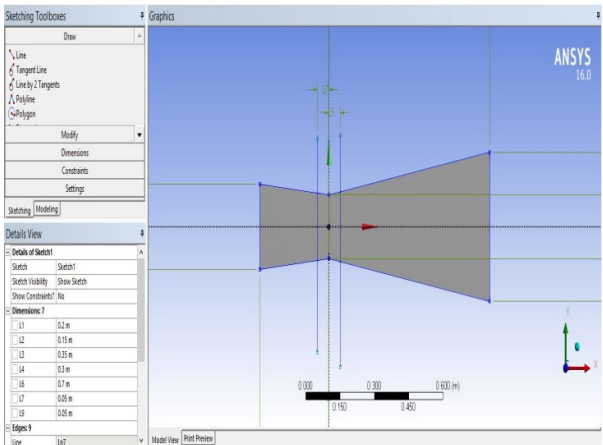
Static Pressure Apr 29, 2018
ANSYS Fluent Release 16.0 (2d, dbns imp, lam)

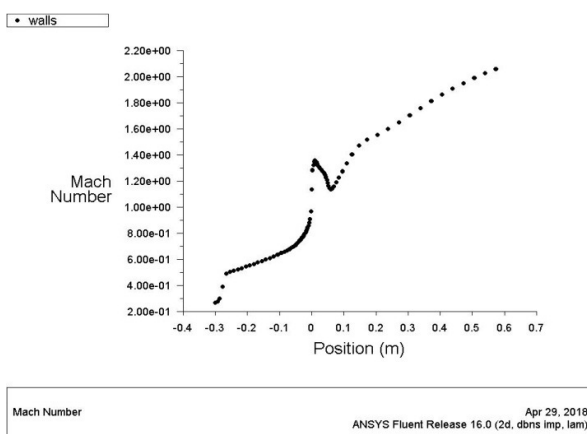
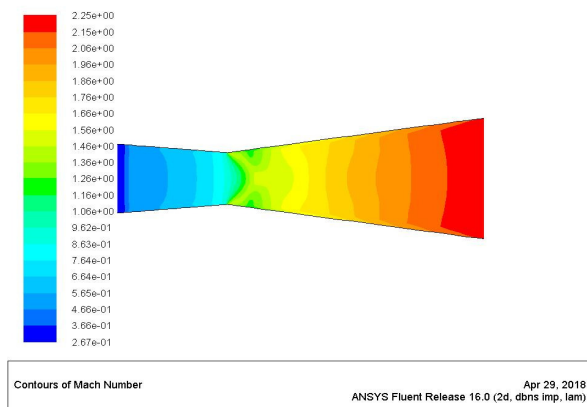
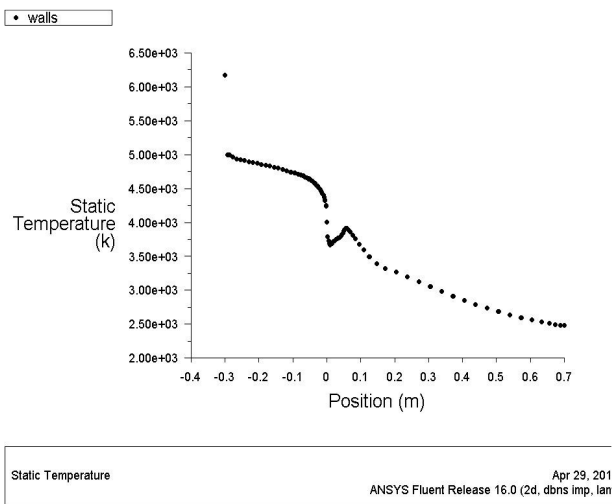


Contours of Mach Number Apr 29, 2018
ANSYS Fluent Release 16.0 (2d, dbns imp, lam)



8.3 Nozzle 3





9. MHD Generator

Magnetohydrodynamic Generator (MHD generator) is a magnetohydrodynamic converter that transforms thermal energy and kinetic energy into electricity. MHD generators are different from traditional electric generators in that

Department of Mechanical Engineering

they operate at high temperatures without moving parts. An MHD generator, like a conventional generator, relies on moving a conductor through a magnetic field to generate electric current. The MHD generator uses hot conductive ionized gas (a plasma) as the moving conductor. There are mainly three types of MHD Generator and they are: -

- Faraday Generator
- Hall Generator
- Disc Generator

Here we have used the Disc Generator for this project.

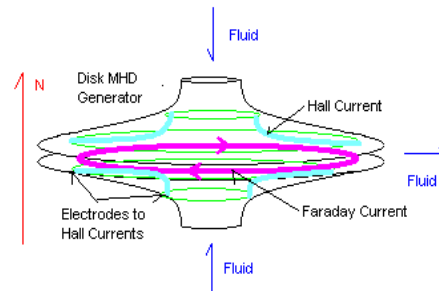


Fig 3: Disc MHD Generator (Courtesy: Wikipedia)

9.1 Disc MHD Generator

The Hall Effect disc generator is the most efficient MHD Generator. This design currently holds the efficiency and energy density records for MHD generation. A disc generator has fluid flowing between the centre of a disc, and a duct wrapped around the edge. The magnetic excitation field is made by a pair of circular Helmholtz coils above and below the disc. The Faraday currents flow in a perfect dead short around the periphery of the disc. The Hall Effect currents flow between ring electrodes near the centre and ring electrodes near the periphery.

Another significant advantage of this design is that the magnet is more efficient. First, it has simple parallel field lines. Second, because the fluid is processed in a disc, the magnet can be closer to the fluid, and magnetic field strength increases as the third power of distance. Finally, the generator is compact for its power, so the magnet is also smaller. The resulting magnet uses a much smaller percentage of the generated power.

9.2 Analysis of the Disk MHD Generator

In the analysis part of the disc MHD Generator we have to find out various data like the maximum current (I_{max}) flowing between the electrodes of the generator, maximum voltage produced in the generator (V_{max}), maximum power produced by the generator (P_{max}) and the efficiency of the MHD Plant.

From the table 7.1 we have obtained that the nozzle 3 has the maximum efficiency among all the three nozzles i.e 65.5%. So the parameters obtained from the nozzle 3 is considered for the calculation of various data related to the

MHD Generator (generally the exit velocity, U_e of the nozzle 2)

Table 6: Parametric values considered/obtained for MHD Generator calculation

Parameters	Corresponding Values(assumed/obtained)
Magnetic Field applied (B)	2 Tesla
Electrical Conductivity (σ)	15 mho/meter
Area of the electrode (A)	1 meter ²
Distance between the electrodes (L)	1 meter
Velocity at nozzle outlet (U_e)(for nozzle 2)	1681.08 meter/sec (obtained from nozzle analysis)

From the data obtained from the above table we can calculate the following:

Maximum Current (I_{max}) :-

$$I_{max} = \frac{B \times \sigma \times A}{2} = \frac{2 \times 15 \times 1}{2} = 15 \text{ amp}$$

Maximum Voltage (V_{max}):-

$$V_{max} = \frac{B \times U_e \times L}{2} = \frac{2 \times 1100.8 \times 1}{2} = 1100.8 \text{ Volt}$$

Maximum Power (P_{max}):-

$$P_{max} = \frac{A \times L \times \sigma \times U_e^2 \times B^2}{4} = \frac{1 \times 1 \times 15 \times 1100.8^2 \times 2^2}{4} = 18.2 \text{ M.Watt}$$

Efficiency of the MHD Plant (ϵ):-

$$\epsilon = \frac{P_{max}}{m_{fuel} \times HHV} = 0.77 \approx 77\%$$

10. Conclusion

In this project we tried to find out the best possible fuel and other mechanical components for the MHD cycle to increase its efficiency. We tried to find out which coal is best suitable for this cycle and which Mach number is suitable for the nozzle in the MHD cycle to give more output with the same amount of energy input for better energy utilization, that is why we compared different Nozzles having different Mach numbers in the open cycle MHD generator. Different important aspects of the nozzles were compared graphically for better results.

Bituminous coal was found to be the most efficient coal for this cycle, therefore the analysis for this coal was done then the heating value was determined, after that flow rates and adiabatic temperatures were calculated. Then came the nozzle, from the comparison among the parameters of the three nozzles the second nozzle was found to be the most suitable one for this cycle. At last the generator analysis was done. Finally we found that from an input of 0.8

kg/sec coal with 20% excess air the cycle will give an output of 42.4 M.Watt power, 1681.08 Volt potential difference, and maximum current of 15 ampere. The overall efficiency of the cycle is approximately 50%.

11. References

- [1] Vishal. D. Dhareppagol, Anand Saurav, The Future Power Generation with MHD Generators Magneto hydro dynamic generation, VP.Dr.P.G.Halakatti College of Engineering & Technology, Bijapur-586103, India.
- [2] Ajith Krishnan R, Jinshah B, Magnetohydrodynamic power Generation, Department of Mechanical Engineering, Government Engineering College, Kozhikode, Kerala.
- [3] Samin Anghaie, Girish Saraph, Innovative Nuclear space power propulsion Institute, University Of Florida, Gainesville, Florida, Project Title: Droplet-Vapor Core Reactors with MHD Power Conversion Units, 1995.
- [4] Zhou Kuo, Sha Ciwen, Yang Aihua and Yin Huiming, Institute of Electrical Engineering, Academia, Bijing, 10080 China.
- [5] Ankur Geete, A.I. Khandwawala, Mechanical Department, S. D. Bansal College of Technology, Indore, Madhya Pradesh, India., Case studies in Thermal Engineering 1 (2013) 17-25.
- [6] Salvatore P. Cicconardi, Alessandra Perna, University of Cassino and Southern Lazio, Via G. di Biasio 43, Cassino, Italy. 68th Conference of the Italian Thermal Machines Engineering Association, ATI2013. ScienceDirect, Energy Procedia 45 (2014) 1305-1314.
- [7] R. Poonthan, S. Anand Kumar Verma, V.S.B. Engineering College, ResearchGate, Article- May 2016.
- [8] M.F.M.A. Majid, Muhamad Al-Hakim Md Apandi, M. Sabri, K. Shahril, Mechanical Section, Universiti Kuala Lumpur Malaysian Spanish Institute, Malaysia., Materials Science and Engineering 114 (2016) 012145.
- [9] Carlo A. Borghi, Motoo Ishikawa, New concepts of MHD power Generation, Dept of Electrical Engineering, University of Bologna, Viale Risorgimento 2 I-40136 Bologna, Italy.
- [10] Sharad Sharma, Sangam Gambhir, International Journal of Computing and Corporate Research, Volume 5 Issue 5 September 2015.
- [11] Bahri Sahin, Ali Kodal, Hasbi Yavuz, Journal of Physics D, Applied Physics, Volume 29, Number 6.
- [12] Muhammad Muneed Khan, Muhammad Aamir Shafi, Zahid Riaz, International Journal of Scientific and Research, Volume 7, Issue 12, December-2016.

[13] J. K. Wright, Physical Principles of MHD generation, Sage Journals, publish date- June 1, 1963.

[14] Fredrick H. Leich, Presented in partial fulfillment of the requirements for the degree of Master of Business Administration, University of Montana, 1971.

[15] S.K.Som, Gautam Biswas, Suman Chakraborty, Introduction to Fluid Mechanics and Fluid Machines, Third edition.

[16]URL: www.electrical4u.com/mhd-generation-or-magneto-hydro-dynamic-power-generation.

[17]URL: www.britannica.com/technology/magnetohydrodynamic-power-generator.

Performance Analysis of a Coal-fired Reheat Regenerative Steam Power Plant

R. Bora

rupshree567@gmail.com

T. K. Gogoi

tapan_g@tezu.ernet.in

Abstract— The objective of the current study is to perform energy and exergy analysis of a coal fired reheat regenerative steam power plant with one reheater, one deaerator and total six numbers of closed feed water heaters (CWHS) (three above and three below the deaerator). In the first part of the study, thermodynamic modelling of the reheat regenerative power plant is done. While simulating, we have considered pressure losses at all the components of the plant to make the analysis more realistic. The results show that the power plant requires a coal burning rate of 15.08kg/s to produce approximately 200 MW of net power with corresponding energy and exergy efficiencies of 40.98% and 38.50%. From the exergy analysis, it has been found that the irreversibility rate is the highest in the boiler compared to the other components of the plant.

Keywords— Coal-fired steam power plant, exergy, irreversibility.

1. Introduction

With the growing population around the World, the energy supply to demand ratio is narrowing down day by day, which is leading to the degradation of the non-renewable resources of energy [1]. The growing demand of power has made the entire scientific community to have closer look at the energy systems. Most of the power plants are designed by the energetic performance criteria based on first law of thermodynamics only. But the real useful energy loss cannot be justified by the first law of thermodynamics, because it does not differentiate between the quality and quantity of energy. It is the second law of thermodynamics which states that all kind of energy is not of the same 'quality' [2]. Hence, the exergetic performance based on the second law of thermodynamics has found as useful method in the design, evaluation, optimization and improvement of thermal power plants.

Over the years many research works have been performed based on exergy analysis [1-7]. Mainly, in these studies, thermodynamic simulation results were compared with the design values of the power plants in order to make comprehensive evaluations and main sources of thermodynamic inefficiencies of each plant has been identified. Often regenerative cycles are employed and a number of heaters are used in thermal power plants in order to preheat boiler feed water to increase the plant efficiency [8-21]. In some of the analyses, the effect of operating parameters such as boiler pressure, condenser pressure, steam flow rate were evaluated. But in most of the above studies, the analysis was done for some fixed operating conditions to find out the energetic and exergetic performance parameters. While designing a reheat regenerative VPC, with a given number of heaters, the operative pressures in the respective heaters cannot be arbitrarily chosen and need to be selected in such a way that it maximizes the plant

output. There is no article in the open literature that analyse a reheat regenerative VPC on this aspect.

In the present analysis, a reheat regenerative VPC is considered with one reheater, one deaerator and total six numbers of closed feed water heaters (CWHS) (three above and three below the deaerator) considering pressure losses in the system components. Energy and exergy analysis have been performed on each component of the plant separately. From the exergy analysis, irreversibility in the boiler was found to be maximum.

2. System Description

Fig. 1 shows the schematic of the coal fired steam power plant. The plant consists of total 20 physical devices which include a boiler, 3 turbines, a condenser, 2 water feed pumps, 6 CWHS, one deaerator and total six throttling valves. The working fluid here is water/steam and the fuel used is coal. The superheated steam produced in the boiler is expanded first to the reheat pressure and is reheated to the original superheated temperature for further expansion in the second ST. Then the superheated steam, after expanding to the condenser pressure enters the condenser and it condenses to water completely.

3. Mathematical Modelling

3.1. Assumptions

The fuel (coal) composition is Carbon (C) 60%, Hydrogen (H) 4%, Oxygen (O) 3%, Nitrogen (N) 2%, Sulfur (S) 3%, Moisture (H₂O) 4% and Ash content 24% [22]. Complete combustion of coal is assumed with flue gas comprising of only carbon dioxide (CO₂), Sulphur dioxide (SO₂), water vapor (H₂O) and Nitrogen (N₂) and hence no Oxygen in the product flue gas. 120% theoretical air is used to oxidize the combustible elements in the fuel. Ash in the flue gas is also neglected. The different assumed parameters are listed in table 1. Here, we have considered pressure drop at all the

different subsystems of the plant, to make our analysis more realistic. Assumed values of pressure drops considered during simulation are listed in table 2.

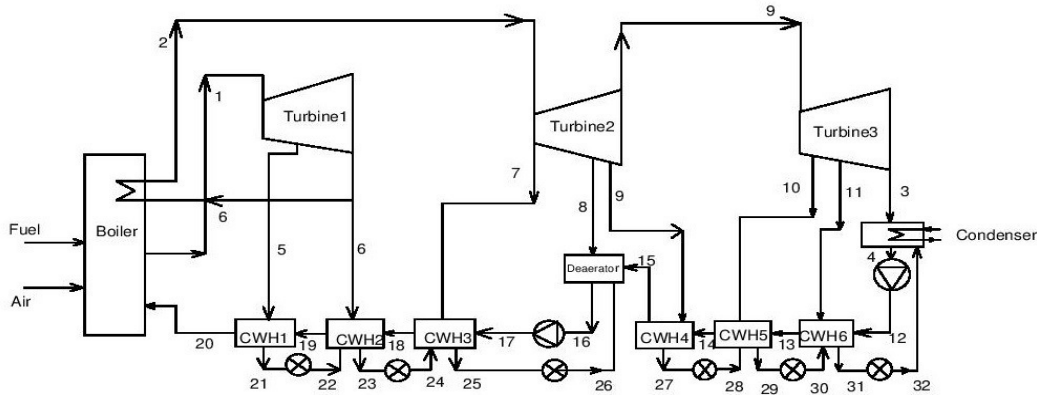


Fig.1 Schematic of the reheat regenerative steam power plant.

TABLE I
ASSUMED VALUES OF PARAMETERS TAKEN FOR SIMULATION

Parameter	Value
Fuel flow rate	15 kg/s
Boiler pressure	167 bar
OWH pressure	10.278 bar
Condenser pressure	0.1 bar
ST inlet temperature	538°C
ST isentropic efficiency	85%
Pump isentropic efficiency	85%
TTD in the CWHs	5°C
Flue gas temperature at the boiler exit	140°C
Temperature of the reference environment	25°C
Condenser inlet water temperature	25°C
Condenser water outlet temperature	35°C

TABLE II
ASSUMED VALUES OF PRESSURE DROPS TAKEN FOR SIMULATION

Component	Pressure drop
Reheater	2%
OWH	3%
CWHs	3%
Condenser	3%
OWH (water side)	1.5%
CWH(water side)	2%

3.2 Topping cycle modelling

For the molar specific heat of the combustion gases, the following temperature dependent model is adopted.

$$\frac{C_p}{R} = a_1 + a_2T + a_3T^2 + a_4T^3 + a_5T^5 \quad (1)$$

The values of the coefficients ($a_1 - a_5$) for the combustion gases are known [24]. Mass flow rate and mass based specific heat of the combustion gases are determined using the same procedure as outlined in [22]. Fuel's lower heating value is calculated as follows [22].

$$LHV_f = - \left[\sum_P n \bar{h}_d^0 - \sum_R n \bar{h}_d^0 \right] \quad (2)$$

The energy lost with the flue gas is calculated using the following equation.

$$\dot{E}_{ex} = \frac{\dot{m}_f}{100} \sum_{i=1}^n n_i \Delta \bar{h}_i \quad (3)$$

Where, $\Delta \bar{h}_i$ is enthalpy change of the i^{th} flue gas product corresponding to the states of flue gas exhaust temperature and the reference temperature.

$$\dot{E}_{ex, f} = \frac{\dot{m}_f}{100} \left[\left\{ LHV_f + 2442 \frac{H_2O}{100} \phi + 9417 \frac{S}{100} \right\} \right] \quad (4)$$

Where,

$$\phi = 1.0437 + 0.1882 \frac{H}{C} + 0.061 \frac{O}{C} + 0.0404 \frac{N}{C} \quad (5)$$

For the details, the articles [22-23] can be referred. Thermodynamic properties of water and steam) are computed using equations taken from IAPWS formulation [25].

For calculating irreversibility of the flue gas ($\dot{E}x_{fg}$), both the chemical and thermo-mechanical exergy are considered. Molar specific chemical exergy of flue gas is calculated from the equation stated below.

$$\dot{E}x_{ch,fg} = RT_0 \sum_i \dot{n}_i \ln \left(\frac{X_i}{X_i^0} \right) \quad (6)$$

Where, X_i is the molar flow rate, and X_i^0 are the mole fractions of the species i in the flue gas product and the reference environment respectively. Thermo-mechanical exergy of the flue gas stream is found out using Eq. (7).

$$\dot{E}x_{m,fg} = \sum_i \dot{n}_i \left[\bar{h}_i(T) - \bar{h}_i(T_0) - T_0 (\bar{s}_i(T) - \bar{s}_i(T_0)) - RT_0 \ln \frac{p}{p^0} \right] \quad (7)$$

The following general mass, energy and exergy balance equations of steady flow processes are applied to find work transfer rate (\dot{W}), heat transfer rate (\dot{Q}) and exergy destruction ($\dot{E}x_d$) rate.

Mass balance:

$$\sum \dot{m}_{in} = \sum \dot{m}_{out} \quad (8)$$

Energy balance:

$$\sum \dot{Q} - \sum \dot{W} = \sum (\dot{m}h)_{in} - \sum (\dot{m}h)_{out} \quad (9)$$

Exergy balance:

$$\sum \dot{E}x_{in} - \sum \dot{E}x_{out} - \dot{Q} \left(1 - \frac{T_0}{T} \right) - \dot{W} - \dot{E}x_d = 0 \quad (10)$$

Where, $\dot{E}x$ is the total exergy, the product of mass flow rate and specific exergy. The total system irreversibility (\dot{I}_{tot}) in the topping cycle is determined by summing up the exergy destruction i.e. $\dot{E}x_d$ (or irreversibility \dot{I}) in all the power cycle components.

4. Results and Discussion

A MATLAB program was developed to simulate the coal-fired system. The operation thermodynamic properties for the various power plant points are given in table 3. This table also represents the exergy rate involved with each component of the plant. The pressures and temperatures in all the 32 points are based on some reference [26]. But here as we have also considered pressure drop throughout the various parts of the plant, hence the pressure of the working fluid at different parts of the plant will change as it moves from the water side to the steam side or vice versa.

In the boiler, air and fuel are entering while the flue gas is leaving the boiler after the combustion of the fuel

in the combustion chamber of the boiler. The fuel will have its chemical exergy (E_f) while the flue gas will have both thermo-mechanical (E_{xgT}) as well as chemical exergy (E_{chf}). Also, the air will have thermo-mechanical exergy (E_{air}). The exergy associated with the boiler are calculated separately while simulating the plant. Those are listed in table 4.

Table IV: Exergy associated with the boiler:

Exergy	Numerical value (kW)
E_{ex}	9060
E_f	32400
E_{xgT}	56800
E_{chf}	345000

Important calculations like work done by the turbines as well as on the pumps, net efficiencies and irreversibility associated with the main components of the plant obtained during simulation are tabulated in table 5.

Table V: With the enthalpies and entropies as inputs, the important outputs obtained:

Outputs	Numerical value
m_s (kg/s)	115.15
LHV (kJ/kg)	32363
Q_{in} (kJ/kg)	2731.7
Q_{lc} (kW)	17387
W_{ST} (kJ/kg)	1152
W_p (kJ/kg)	23.56
W_{net} (kJ/kg)	1128.4
P (MW)	129.94
η_{boiler} (%)	79.5
η (%)	40.15

Considering the pressure drops at various points throughout the whole plant, we have also simulated the plant for waterside and steam side pressure drops separately. The results obtained for all the heaters are tabulated in table 6.

Table VI: Water side and steam side pressure drops for all the CWHs:

Components	Waterside pressure drop	Steam side pressure drop
CWH1	0.258	0.114
CWH2	0.262	0.116
CWH3	0.266	0.078
CWH4	0.03	0.023
CWH5	0.031	0.012
CWH6	0.032	0.004

Table 3 The operation thermodynamic properties and exergy of the system corresponding to figure 1:

Point	P (bar)	T ($^{\circ}\text{C}$)	m (kg/s)	h (kJkg $^{-1}$)	s (kJkg $^{-1}$ K $^{-1}$)	E (kW)
1	167	538	115.15	3398.61	6.41	1490.50
2	34.72	538	98.81	3537.93	7.27	1374.40
3	0.15	53.97	76.77	2488.01	7.66	205.77
4	0.14	53.34	92.06	223.30	0.74	5.20
5	57.11	378.75	115.15	3128.92	6.48	1198.65
6	38.57	328.17	108.20	3041.61	6.51	1103.66
7	19.55	455.15	98.810	3369.97	7.31	1194.19
8	10.27	370.84	95.43	3201.92	7.35	1012.26
9	5.96	306.10	92.06	3074.82	7.39	873.52
10	2.55	216.91	87.14	2902.45	7.46	682.35
11	0.87	122.11	82.16	2722.15	7.54	477.56
12	10.98	53.43	92.06	224.59	0.74	6.300
13	10.66	89.45	92.06	375.46	1.18	26.51
14	10.3	121.48	92.06	510.66	1.54	55.17
15	10.05	151.63	92.06	639.63	1.85	90.23
16	9.76	178.85	115.15	758.11	2.12	128.09
17	179.86	181.99	115.15	780.64	2.13	148.30
18	177.20	204.21	115.15	877.94	2.34	183.22
19	174.59	241.42	115.15	1046.23	2.68	250.14
20	172.01	266.08	115.15	1163.22	2.90	300.75
21	55.97	271.08	6.950	1190.64	2.98	304.87
22	37.41	246.42	6.95	1190.64	2.76	372.08
23	37.41	246.42	16.34	1068.38	2.76	249.82
24	18.77	209.21	16.34	1068.38	2.41	352.20
25	18.77	209.21	19.71	894.12	2.41	177.94
26	9.76	178.85	19.71	894.12	2.12	264.10
27	5.670	156.63	4.91	660.97	1.90	96.34
28	2.43	126.48	4.91	660.97	1.59	189.30
29	2.43	126.48	9.90	531.37	1.59	59.70
30	0.82	94.45	9.90	531.37	1.24	165.04
31	0.82	94.45	15.29	395.73	1.24	29.40
32	0.14	53.34	15.29	395.73	0.74	177.64

5. Conclusions

The exergy analysis was basically done on the proposed plant to quantify the losses occurring at the various subsystems of the plant. In the first part of the study, we have modelled the reheat regenerative plant using six numbers of closed feed water heaters and one deaerator. The simulation was done in MATLAB. While simulating, we have considered pressure losses at all the

salient points of the plant to make the analysis more realistic. On simulation, we got that boiler has the highest irreversibility of 123930 kW followed by turbine and condenser with 13531 kW and 12546 kW. Also, from this analysis, it is evident that only 5% of exergy has lost in the condenser.

References

- [1] Kaushik, S. C., Reddy, V. S., and Tyagi, S. K., 2011, Energy and exergy analyses of thermal power plants: A review, *Renewable and Sustainable Energy Reviews*, 15(4), pp:1857–1872..
- [2] Hasan H.E, Ali V.A., Burhanettin, Ahmet D., Suleyman H.S., Bahri S., Ismail T., Cengiz G., Selcuk A., 2009, Comparative energetic and exergetic performance analyses for coal-fired thermal power plants in Turkey, *International Journal of Thermal Sciences*, 48, pp. 2179 - 86.
- [3] Oktay, Z., 2009, Investigation of coal-fired power plants in Turkey and a case study, *Applied Thermal Engineering*, 29, pp. 550–557.
- [4] Regulagadda, P., Dincer, I., and Naterer, G. F., 2010, Exergy analysis of a thermal power plant with measured boiler and turbine losses, *Applied Thermal Engineering*, 30, pp. 970–976.
- [5] Dincer I, Rosen M.A., 2007, Exergy ,energy, environment and sustainable development. *Elsevier*; 30, pp. 456-567.
- [6] Aljundi, I. H., 2009, Energy and exergy analysis of a steam power plant in Jordan, *Applied Thermal Engineering*, 29, pp. 324–328.
- [7] Erdem, H. H., Akkaya, A. V., Cetin, B., Dagdas, A., Sevilgen, S. H., Sahin, B., Teke, I., Gungor, C., and Atas, S. , 2009, Comparative energetic and exergetic performance analyses for coal-fired thermal power plants in Turkey, *International Journal of Thermal Sciences*, 48, pp. 2179–2186.
- [8] Habib M. A, Said S. A. M. , Al-Bagawi J. J. ,2007, Thermodynamic performance analysis of the Ghazlan power plant, *Energy*, 20, pp. 1121 - 30.
- [9] Dincer, I. and Al-Muslim, H., 2001, Thermodynamic analysis of reheat cycle steam power plants, *International Journal of Energy Research*, 25, pp. 727–739.
- [10] Habib, M. A. and Zubair, S. M., 1992, Second-law-based thermodynamic analysis of regenerative-reheat Rankine-cycle power plants, *Energy*, 17, pp. 295–301.
- [11] Kopac, M. and Hilalci, A., 2007, Effect of ambient temperature on the efficiency of the regenerative and reheat Catalagzi power plant in Turkey, *Applied Thermal Engineering*, 27, pp. 1377–1385.
- [12] Tsatsaronis G, Lin L, Pisa J., 1993, Exergy costing in Exergoeconomics, *J Energy –ASME*, 115, pp. 9–16.
- [13] Bejan A., Tsatsaronis G., Moran M., 1996, Thermal design and optimization, 1st ed., New York: Wiley.
- [14] Tsatsaronis G., Moran M.J., Exergy-aided cost minimization, *Energy Convers Manage* 1997,38, pp.1535–42.
- [15] Tsatsaronis G., Ho-Park M., 2002, On avoidable and unavoidable exergy destructions and investment costs in thermal systems, *Energy Convers Manage*, 43, pp. 1259–70.
- [16] Zhang, C., Wang, Y., Zheng, C., and Lou, X., 2006, Exergy cost analysis of a coal fired power plant based on structural theory of thermoeconomics, *Energy Conversion and Management*, 47, pp. 817–843.
- [17] Ameri, M., Ahmadi, P., and Hamidi, A. , 2009, Energy, exergy and exergoeconomic analysis of a steam power plant: A case study, *International Journal of Energy Research*, 33, pp. 499–512.
- [18] Sahoo, P. K., Exergoeconomic analysis and optimization of a cogeneration system using evolutionary programming, *Applied Thermal Engineering*, 28, pp. 1580–1588.
- [19] Khaljani, M., Saray, R. K. and Bahlouli, K., 2015, Comprehensive analysis of energy, exergy and exergo-economic of cogeneration of heat and power in a combined gas turbine and organic Rankine cycle, *Energy Conversion and Management*, 97, pp.154–165.
- [20] Valdes, M., Duran, M. D., Rovira, A. , 2011, Thermoeconomic optimization of combined cycle gas turbine power plants using genetic algorithms, *Applied Thermal Engineering*, 23, pp. 2169–2182.
- [21] Quoilin, S., Declaye, S., Tchanche, B.F. and Lemort, V., 2011, Thermo-economic optimization of waste heat recovery Organic Rankine Cycles, *Applied Thermal Engineering*, 31, pp. 2885–2893.
- [22] Gogoi, T.K. and Talukdar, K., 2014, Exergy based parametric analysis of a combined reheat regenerative thermal power plant and water–LiBr vapor absorption refrigeration system, *Energy Conversion and Management*, 83, pp.119–132.
- [23] Gogoi, T.K. and Talukdar, K., 2014, Thermodynamic analysis of a combined reheat regenerative thermal power plant and water–LiBr vapour absorption refrigeration system, *Energy Conversion and Management*, 78, pp. 595-610.
- [24] Moran, M.J. and Shapiro, H.N., 2005, *Fundamental of Engineering Thermodynamics*, Singapore: John Wiley & Sons, 4th edition.
- [25] W. Wagner, J. R. Cooper, A. Dittmann, J. Kijima, H.-J. Kretzschmar, A. Kruse, R. Mares, K. Oguchi, H. Sato, and I. Stocker, 2000, The IAPWS Industrial Formulation 1997 for the thermodynamic properties of water and steam, *Journal of Engineering for Gas Turbines and Power* 122, pp. 150–81.
- [26] Tsatsaronis G, Pisa J., 1994, Exergoeconomics evaluation and optimization of energy systems application to the CGAM problem, *Energy—The International Journal*, 19, pp. 287–296.

Laser Forming Mechanism: A Review

Joy Nondy

joynondy21.jn@gmail.com

P.M. Kalita

paragmk@tezu.ernet.in

P.P. Dutta

polashd@tezu.ernet.in

Abstract— Laser forming plastically deforms the material by means of a laser beam with or without the application of mechanical loads. It is used for bending of sheets and tubes and for producing complex shapes. A number of researchers studied the process and suggested the strategies for process design, control and optimisation strategies. There is still need for understanding the physics of laser forming process and the parameters controlling the mechanism.

Keywords: Laser , Forming, Bending, Temperature gradient

1. Introduction

Laser forming is a process of deforming a work piece using defocused laser radiation, without the use of dies or tools. The defocused laser radiation induces thermal stresses, which plastically deforms the work piece. The laser beam can be easily transferred by a fibre optical cable, which makes the process suitable for the applications where mechanical tools are not accessible. This non-contact nature of laser forming process gives the advantage of no tool-wear as well as high level of flexibility. The laser beam can be focused at a small area thus making it suitable for processing of small components. Laser forming process can be used to bend thin sheets, foils and tubes for a wide range of materials such as metals, non-metals, plastics, ceramic and composites. Even brittle material like glass can also be deformed using laser forming process. One more advantage with this process is that small and precise bend angle can be obtained which is not possible with conventional method due to spring back effect. Since last two decades, several papers have been published on laser forming process where focus was to understand the underlying physics of the process and produced various models for the prediction of temperature profile and bend angle.

Some of the models are analytical and some are based on numerical methods such as finite element method (FEM). Based on temperature profile, Shen and Vollertsen [7] presented a literature review for the modelling of laser forming where laser forming mechanism is classified into three types *viz.*, temperature gradient mechanism (TGM), buckling mechanism (BM) and upsetting mechanism (UP). TGM and BM are responsible for bending of work piece and UP is used for shortening and thickening of work piece. Out of three mechanisms, TGM is widely used. It can give a bend angle of 0.1°C to 3°C for a single laser scan.

Vollertsen [8] derived an expression for the bending angle for TGM. His model does not include the effect of yield stress of material. A mathematical model was developed by kyrsanidiet *al.* [9] who consider non-uniform temperature distribution throughout the thickness of the plate due to the developed plastic strains. This model,

plastic deformation is generated only during heating, while during cooling the plate undergoes only elastic deformation. The model is valid for TGM as well as BM. Recently, Lambiase [10] proposed expression for the bending angle based on assumption of elastic-bending theory without taking into account plastic deformation during heating and cooling phases.

2. Mechanism

Localised heating of the work piece, which induces thermal stress and deforms the work piece plastically. The laser forming process is governed by three different mechanism types *viz.*, temperature gradient mechanism (TGM), buckling mechanism (BM) and upsetting mechanism (UP) based on the temperature profile developed on the plate.

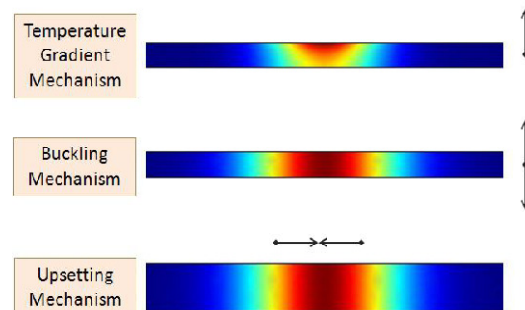


Fig. 1 Temperature profile for along the thickness for TGM, BM and UP. The direction of arrow depicts bend direction.

2.1 Temperature Gradient Mechanism

A step thermal gradient is generated along the thickness, causing the softer upper material to plastically deform, yielding a bend angle of 0.1°C to 3°C per pass. In order to establish the required thermal gradient, the depth of heating must be relatively small compared to the sheet

thickness, this being achieved through a suitable combination of traverse speed, spot size and laser power.

Eideh *et al.* [6] carried a numerical investigation of laser forming on a D36 shipbuilding steel sheet for a moving and stationary heat source. The relationship obtained from the analysis is further used for understanding TGM better.

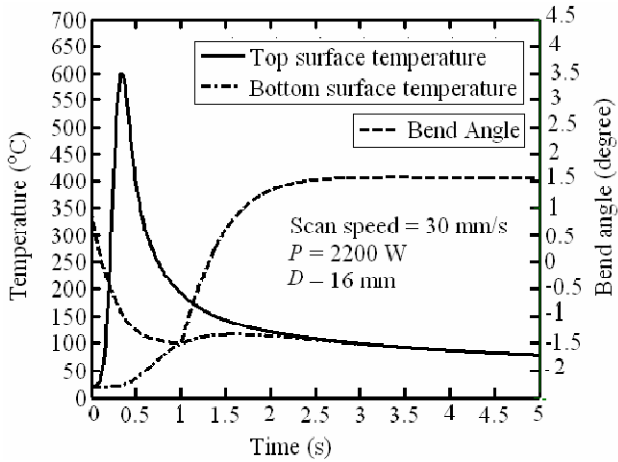


Fig. 2 Temperature and bend angle variation during laser forming process on a D36 shipbuilding steel sheet.

Figure 2 shows the variation of temperature and bend angle for a moving heat source on a D36 shipbuilding steel. It is observed that at the initial stage of heating the sheet bends away from the laser, which is known as counter bending and during cooling the sheet bends towards the laser.

2.2 Buckling Mechanism

The BM occurs when the temperature difference between the top surface and bottom surface of the work piece is negligible. Large beam diameters relative to work piece thicknesses coupled with low traverse speeds typically results in elastic-plastic buckling, which can cause deformation towards or away from the beam. The conditions which facilitate the BM are thin work piece of high thermal conductivity, large beam diameter and slow scanning speed. Bend angle of 1° to 15° can be obtained in a BM dominated operation for a single laser scan. In compare to TGM, BM gives more bend angle and counter bending is not observed in BM unlike TGM. In BM the direction of bend is not fixed and it is determined by the pre curvature of the sheet, external force and internal stress.

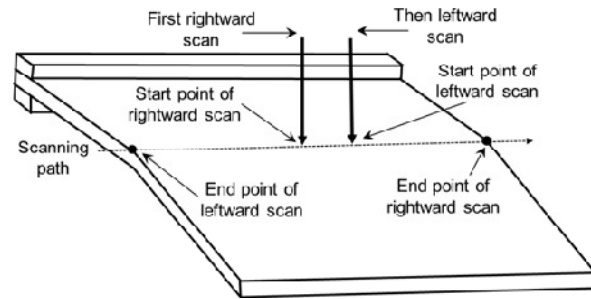


Fig. 3 Irradiation scheme for laser bending direction in BM

Li and Yao[3] postulated an irradiation scheme as shown in figure 3. In this scheme, the laser starts from the middle of the work piece instead of edges. First rightward and then leftward scanning is done from the middle. This scheme gives an downward bending away from the laser source. Shi et al[4] proposed a conditional inequality to determine whether an operation is BM dominated or not.

$$\frac{pd^{1/2}}{h^2V^{1/2}} \geq \frac{\eta\pi^{7/2}k^{1/2}\rho^{1/2}c_p^{1/2}}{41.52(1+\mu)A\alpha_{th}} \quad (1)$$

where $P, d, h, V, \eta, k, \rho, c_p, \mu, A$ and α_{th} are laser power, beam diameter, sheet thickness, scan speed, correction factor, thermal conductivity, density, specific heat, Poisson's ratio, absorptivity and coefficient of thermal expansion, respectively. It can also be determined by using Fourier number which is given by

$$F_0 = \alpha_d d / h^2 V \quad (2)$$

where α_d, h, d and V are thermal diffusivity, sheet thickness, beam diameter and scanning speed. The smaller value of Fourier number indicates that TGM is dominated and small value of Fourier number indicates BM is dominated. Chen et al[5] used 160 W diode laser for bending of low carbon sheet of thickness 0.25 mm, 0.51 mm and 0.79 mm, respectively. It is observed that BM is dominated and gives the largest bending angle when beam diameter to sheet thickness aspect ratio was four. For aspect ratio less than two, TGM and BM both contribute to bend angle.

2.3 Upsetting Mechanism

The UM is used for shortening of small frames, tubes and pipe bending for various cross section. In this mechanism, the work piece shortens and thickens in a heated region and therefore it is also called as shortening mechanism. The process conditions for UM are similar to BM as in both case the temperature gradient along the

thickness direction is negligible. The only difference is that the work piece is thick and beam diameter is lesser than the work piece thickness. Ideally, homogeneous heating is applied throughout the thickness of the work piece. Thermal expansion in the irradiated area occurs as a result of this heating, reducing the flow stress of the material. As, in the TGM and BM, this thermal expansion is restricted by the cold surrounding material and providing the thermal strain

induced is sufficiently high, this causes compressive stresses to develop, resulting in plane shortening of the work piece.

3. Effects of process parameters on mechanism

As discussed in the previous subsections, the selection of process parameters for a given work piece geometry has a controlling effect on the mechanism by which deformation occurs in the laser forming process.

TABLE 1

LASER FORMING MECHANISM PROCESS CHARECTERS

Method	Scanning Speed	Spot Size	Laser Power	Section Thickness	Bend Direction
TGM	High	Small	High	Thin	Out of plain towards beam
BM	Low	Large	Low	Thin	Out of plain either direction
UM	Low	Large	Low	Thick	In-plain shortening

As highlighted in Table 1, laser power, scanning speed, spot size and power are main process parameters in laser forming. Thus, by controlling the process parameters desired laser forming mechanism can be made predominated and the desired results can be obtained.

4. Conclusion

During last two decades, a large number of papers have appeared on experimental and theoretical studies on laser forming. However, the physics involved in the process is still not being studied extensively. Thus, in this paper, an extensive and comprehensive review on the literature available on the mechanism of laser forming process is presented.

References

- [1] Hu, Z. and Kovacevic,R.,2002, Study of Microstructures in Laser bending, *International Journal of Machine Tools & Manufacture*, Vol, 42:1427-1439.
- [2] Shi,Y., Shen,H.,Yao,Z. and Hu,J., 2007a, Temperature gradient mechanism in laser forming of thin plates, *Optics & Laser Technology*, Vol.39,No.4,pp.858-863.
- [3] Li,W. and Tao,Y.L.,2001a,Laser bending of tubes: mechanism analysis and prediction, *Journal of Manufacturing Science and Engineering*, Vol. 123, No.4, pp.6774-681.
- [4] Shi,Y., Yao,Z., Shen,H. and Hu,J.,2006b, Research on the mechanism of laser forming for the metal plate, *International Journal of Machine Tools and Manufacture*, Vol.46,No.12,pp.1689-1697.
- [5] Chen, J., Yao, Y.L., 2004, Process design of laser forming for three-dimensional thin plates, *Journal of Material Processing Technology*, Vol.152:62-65.
- [6] Eideh, A., Dixit, U.S.,Echempati, R.,2014, A simple analytical model of laser bending, *5th International & 26th All India Manufacturing Technology, Design and Research Conference (AIMTDR 2014) December 12th-14th, 2014, IIT Guwahati, Assam, India*
- [7]Shen,H. and Vollertsen,F.,2009,Modelling of laser forming-An review, *Progressional Material Science*, Vol.46,pp.834-840.
- [8] Vollertsen. F., 1994, An analytical model for laser bending, *Laser in Engineering*, Vol.2,pp.261-276
- [9] Kysanidi.A.K., Kermanidis,T.B. and Pantelakis,S.G.,2000, An analytical model for the predictions of distortions caused by laser forming process, *Journal of Materials Processing Technology*, Vol.104,pp.94-102.
- [10] Lambiase,F.,(2012), An analytical model for evaluation of bending angle is laser forming of metal sheets, *Journal of Material Engineering and performance*, Vol.21,pp.2044-2052

